

# Probing a GRB progenitor at a redshift of $z=2$ : a comprehensive observing campaign of the afterglow of GRB 030226<sup>1</sup>

S. Klose<sup>1</sup>, J. Greiner<sup>2</sup>, A. Rau<sup>2</sup>, A. A. Henden<sup>3</sup>, D.H. Hartmann<sup>4</sup>, A. Zeh<sup>1</sup>, C. Ries<sup>5</sup>, N. Masetti<sup>6</sup>, D. Malesani<sup>7</sup>, E. Guenther<sup>1</sup>, J. Gorosabel<sup>8,9</sup>, B. Stecklum<sup>1</sup>, L.A. Antonelli<sup>10</sup>, C. Brinkworth<sup>11</sup>, J.M. Castro Cerón<sup>8</sup>, A.J. Castro-Tirado<sup>9</sup>, S. Covino<sup>12</sup>, A. Fruchter<sup>8</sup>, J.P.U. Fynbo<sup>13,14</sup>, G. Ghisellini<sup>12</sup>, J. Hjorth<sup>14</sup>, R. Hudec<sup>15</sup>, M. Jelínek<sup>15</sup>, L. Kaper<sup>16</sup>, C. Kouveliotou<sup>17</sup>, K. Lindsay<sup>4</sup>, E. Maiorano<sup>6,19</sup>, F. Mannucci<sup>20</sup>, M. Nysewander<sup>21</sup>, E. Palazzi<sup>6</sup>, K. Pedersen<sup>14</sup>, E. Pian<sup>6,22</sup>, D. E. Reichart<sup>21</sup>, J. Rhoads<sup>8</sup>, E. Rol<sup>22</sup>, I. Smail<sup>23</sup>, N.R. Tanvir<sup>24</sup>, A. de Ugarte Postigo<sup>9</sup>, P.M. Vreeswijk<sup>25</sup>, R.A.M.J. Wijers<sup>16</sup>, E.P.J. van den Heuvel<sup>16</sup>

Received: 4 June 2004 / Accepted: 14 July 2004

---

- <sup>1</sup> Thüringer Landessternwarte Tautenburg, Sternwarte 5, 07778 Tautenburg, Germany
- <sup>2</sup> Max-Planck-Institut für extraterrestrische Physik, 85741 Garching, Germany
- <sup>3</sup> U. S. Naval Observatory/Universities Space Research Association, Flagstaff Station, Flagstaff, AZ 86001, USA
- <sup>4</sup> Clemson University, Department of Physics and Astronomy, Clemson, SC 29634-0978, USA
- <sup>5</sup> Wendelstein-Observatorium, Universitätssternwarte, 81679 München, Germany
- <sup>6</sup> Istituto di Astrofisica Spaziale e Fisica Cosmica, CNR, Sez. di Bologna, Via Gobetti 101, 40129 Bologna, Italy
- <sup>7</sup> International School for Advanced Studies (SISSA-ISAS), via Beirut 2-4, I-34014 Trieste, Italy
- <sup>8</sup> Space Telescope Science Institute, 3700 San Martin Drive, Baltimore, MD 21218-2463, USA
- <sup>9</sup> Instituto de Astrofísica de Andalucía (IAA-CSIC), Apartado de Correos, 3.004, E-18.080 Granada, Spain
- <sup>10</sup> INAF, Osservatorio Astronomico di Roma, Monteporzio Catone, Italy
- <sup>11</sup> School of Physics and Astronomy, University of Southampton, Highfield, Southampton SO17 1BJ, UK
- <sup>12</sup> INAF, Osservatorio Astronomico di Brera, via E. Bianchi 46, I-23807 Merate (Lc), Italy
- <sup>13</sup> Department of Physics and Astronomy, University of Aarhus, Ny Munkegade, 8000 Aarhus C, Denmark
- <sup>14</sup> Astronomical Observatory, University of Copenhagen, Juliane Maries Vej 30, 2100 Copenhagen, Denmark
- <sup>15</sup> Astronomical Institute of the Czech Academy of Sciences, 25165 Ondrejov, Czech Rep.
- <sup>16</sup> University of Amsterdam, Kruislaan 403, 1098 SJ Amsterdam, The Netherlands
- <sup>17</sup> NSSTC, SD-50, 320 Sparkman Drive, Huntsville, AL 35805, USA
- <sup>18</sup> Institute of Astronomy, University of Cambridge, Madingley Road, CB3 0HA Cambridge, UK
- <sup>19</sup> Dipartimento di Astronomia, Università di Bologna, via Ranzani 1, 40129 Bologna, Italy
- <sup>20</sup> IRA/CNR, Sezione di Firenze, Largo E. Fermi 5, I-50125 Florence, Italy
- <sup>21</sup> University of North Carolina, Chapel Hill, NC, USA
- <sup>22</sup> INAF, Osservatorio Astronomico di Trieste, Via Tiepolo 11, 34131 Trieste, Italy
- <sup>23</sup> Institute for Computational Cosmology, Department of Physics, University of Durham, South Road, Durham DH1 3LE, UK
- <sup>24</sup> Department of Physical Sciences, University of Hertfordshire, College Lane, Hatfield Herts, AL10 9AB, UK
- <sup>25</sup> European Southern Observatory, Alonso de Córdova 3107, Vitacura, Casilla 19001, Santiago 19, Chile

## ABSTRACT

We report results from a comprehensive follow-up observing campaign of the afterglow of GRB 030226, including VLT spectroscopy, VLT polarimetry, and *Chandra* X-ray observations. In addition, we present BOOTES-1 wide-field observations at the time of the occurrence of the burst. First observations at ESO started 0.2 days after the event when the GRB afterglow was at a magnitude of  $R \sim 19$  and continued until the afterglow had faded below the detection threshold ( $R > 26$ ). No underlying host galaxy was found. The optical light curve shows a break around 0.8 days after the burst, which is achromatic within the observational errors, supporting the view that it was due to a jetted explosion. Close to the break time the degree of linear polarization of the afterglow light was less than 1.1%, which favors a uniform jet model rather than a structured one. VLT spectra show two absorption line systems at redshifts  $z = 1.962 \pm 0.001$  and at  $z = 1.986 \pm 0.001$ , placing the lower limit for the redshift of the GRB close to 2. We emphasize that the kinematics and the composition of the absorbing clouds responsible for these line systems is very similar to those observed in the afterglow of GRB 021004. This corroborates the picture in which at least some GRBs are physically related to the explosion of a Wolf-Rayet star.

*Subject headings:* Gamma rays: bursts – Stars: Wolf-Rayet

## 1. Introduction

Understanding the nature of GRB progenitors remains a primary focus in GRB research. The spectroscopic identification of supernova (SN) light underlying the afterglows of the nearby bursts 030329 (Hjorth et al. 2003a; Kawabata et al. 2003; Matheson et al. 2003; Stanek et al. 2003) and 031203 (Malesani et al. 2004) convincingly demonstrated that core-collapse supernovae are physically related to long-duration GRBs. In most cases, however, GRB-SNe are too faint at their suspected maximum light (cf. Zeh et al. 2004) to confirm their appearance via spectroscopic observations. Revealing the nature of a GRB progenitor by indirect methods thus remains an important approach, in addition to an understanding of the afterglows themselves. In this context of particular interest is the fine structure detected

---

<sup>1</sup>Based on observations collected at the European Southern Observatory, La Silla and Paranal, Chile (ESO Programmes 70.D-0523 and 70.D-0531).

in two of the best monitored afterglow light curves (GRB 021004: e.g., Bersier et al. 2003; GRB 030329: e.g., Lipkin et al. 2004) and the kinematics of absorbing clouds revealed in early-time spectra of the afterglows of GRB 020813 and 021004 (for a discussion see Chevalier et al. 2004; Mirabal et al. 2003; and Schaefer et al. 2003), since both features could be signatures of the physical conditions in the GRB environment. Here we report the results of our comprehensive observing campaign of the afterglow of GRB 030226. Even though the afterglow light curve started faint and faded rapidly, which did not allow us to monitor its evolution in great detail, our early-time spectra do reveal strong spectral similarities between the afterglow of GRB 030226 and those of GRB 020813 and 021004.

GRB 030226 was discovered by the *HETE-2* satellite on 2003 February 26.15731 UT (3:46 UT) with a duration in excess of 100 seconds and a peak flux and fluence in the 30-400 keV band of  $\sim 1.2 \times 10^{-7}$  erg cm $^{-2}$  s $^{-1}$  and  $5.7 \times 10^{-6}$  erg cm $^{-2}$ , respectively (Suzuki et al. 2003). The optical counterpart was detected  $\sim 2.5$  hours later (Fox et al. 2003, 2004) at a magnitude  $R \sim 18.5$  (Garnavich et al. 2003) at coordinates (J2000) R.A. = 11<sup>h</sup> 33<sup>m</sup> 04<sup>s</sup>.92; Decl. = +25° 53' 55".6 (Price et al. 2003a; von Braun et al. 2003), well within the *HETE-2* Wide Field X-ray monitor (WXM) and Soft X-ray Camera (SXC) error boxes. No optical emission coincident in time with the GRB prompt event was detected (Castro-Tirado et al. 2003; § 4.2). A subsequent *Chandra* observation led to the detection of the X-ray afterglow at a position consistent with that of the optical transient, thus confirming its association with GRB 030226 (Pedersen et al. 2004a).

## 2. Observations and data reduction

Imaging of the central part of the SXC error circle in  $J_s, H, K_s$  began  $\sim 4.5$  hrs after the burst using VLT/ISAAC at ESO Paranal. Simultaneously, imaging in the optical in  $BVR$  was performed using the ESO NTT telescope at La Silla equipped with the multi-purpose instrument EMMI. Also, the 3.8-m United Kingdom Infra-Red Telescope (UKIRT) at Mauna Kea, Hawaii, started observing the GRB afterglow 6 hours after the burst using the UKIRT Fast-Track-Imager (UFTI). Further imaging was performed during the following nights with the ESO NTT telescope equipped with the SUpperb Seeing Imager (SuSI2). Additional data were obtained with the Wendelstein 80-cm telescope near Munich, Germany (using the direct imaging CCD camera MONICA), the 2.5-m Nordic Optical Telescope (NOT) equipped with the Andaluc a Faint Object Spectrograph and Camera ALFOSC, the 1.0-m Jacobus Kapteyn Telescope (JKT), and the Italian 3.5-m Telescopio Nazionale Galileo TNG, using the focal reducer instrument DOLORES (all at La Palma, Spain), the Tautenburg 1.34-m Schmidt telescope equipped with prime focus 4k  $\times$  4k CCD camera, the Asiago 1.8-m

telescope equipped with the AFOSC camera, UKIRT, and the 8-m Gemini South telescope at Cerro Pachón, Chile. The data base, and the derived magnitudes (not corrected for Galactic extinction;  $E(B - V) \approx 0.02$  mag, Schlegel et al. 1998) are summarized in Table 2. These magnitudes supersede those obtained by this collaboration and published in the GCN Circular archive.

Regular observations of the sky were also acquired by the wide-field cameras of the BOOTES project (Castro-Tirado et al. 1999) at the BOOTES-1 astronomical station in Mazagón, Spain. The GRB 030226 location was serendipitously imaged in a simultaneous, unfiltered frame (180 s exposure time) taken on 03:45:16 - 03:48:16 UT. Additional images were available prior to and following the event.

## 2.1. Photometry

After the normal image processing steps (flatfielding, stacking), all stars were extracted using DAOPHOT as implemented in IRAF<sup>2</sup>. Point-spread-function (PSF) fitting was used to derive the brightnesses of the afterglow and comparison stars. PSF stars were carefully selected by first inspecting the deeper, higher resolution images to ensure that no background contamination was present and that all objects were stellar. After extraction, ensemble differential photometry was performed using comparison stars chosen from the field photometry file provided by Henden (2003). Typically four to six comparison stars were used, depending on the depth of the image and the bandpass. No transformations were made to the standard Johnson-Cousins system, but comparison stars were chosen to reduce transformation effects whenever possible.

For the reduction of the near-infrared (NIR) frames ESO’s *eclipse* package was used (Devillard 2002). Photometric calibration of the ISAAC field was performed by the observation of the UKIRT standard star FS 136 (Hawarden et al. 2001) with the VLT. Airmass corrections were applied according to the coefficients provided on ESO’s Web pages (in units of mag airmass<sup>-1</sup>):  $k_J=0.06$ ,  $k_H=0.06$ ,  $k_K=0.07$ . An independent calibration of the UKIRT  $K$ -band data, made using the standard star FS 130 (Hawarden et al. 2001), is in good agreement with the one described above.<sup>3</sup> Next we deduced the following magnitudes for the brightest

---

<sup>2</sup>IRAF is distributed by the National Optical Astronomical Observatories, which is operated by the Associated Universities for Research in Astronomy, Inc., under contract to the National Science Foundation.

<sup>3</sup>Following the detailed photometric work performed by Labbé et al. (2003) on the *Hubble Deep Field South*, we assumed that the ISAAC  $J_s, H, K_s$  filters match the faint NIR standard star system (Persson et al. 1998). We also refer the reader to Labbé et al. (2003; their section 2.1) for more details on the  $J_s$  and

point-like object close to the optical transient (marked “Ref” in Fig. 1) at R.A. (J2000) = 11<sup>h</sup> 33<sup>m</sup> 04<sup>s</sup>.27, Decl. (J2000) = 25° 54′ 22″:  $J_s = 17.10 \pm 0.10$ ,  $H = 16.54 \pm 0.10$ ,  $K_s = 16.44 \pm 0.05$ <sup>4</sup>. This calibration was confirmed with independent observations using the Calar Alto 3.5-m telescope equipped with the Omega Prime NIR camera on March 6, 2004.

## 2.2. VLT spectroscopy

The early report of the discovery of the GRB afterglow by Fox et al. (2003) allowed rapid spectroscopic observations of the optical transient, performed only 5 hrs after the burst, on 2003 Feb 26, 08:52–09:07 UT, with VLT Yepun/FORS2. A 900 s exposure using the 300V grism was obtained when the afterglow was at a magnitude of  $B = 19.8$ . Using a 1″0 slit, the 3.3 Å/pixel scale leads to a resolution of 13 Å (FWHM, 870 km/s at  $\lambda=4500$  Å) at 0″9–1″1 seeing. A second spectroscopic run was performed one night later, on 2003 Feb 27, 07:35–09:08 UT, using VLT Antu/FORS1 equipped with the 600B grism. Five exposures, each one lasting 900 s, were taken at a time when the afterglow had a magnitude of  $B = 21.7$ . The 1.2 Å/pixel scale gave a resolution of 7 Å (FWHM, 470 km/s at  $\lambda=4500$  Å) at 1″0–1″2 seeing with a 1″3 slit. Flatfield and bias correction was applied in the usual way using IRAF. Background subtraction was performed and the wavelength calibration was done using HgCdHe and HgCdHe+Ar calibration lamps. The spectra were corrected for achromatic slit losses following the procedure described in Vreeswijk et al. (2004). The standard stars LTT 6248 (spectral type A) and BD +33°2642 (spectral type B2 IV) were observed in order to flux-calibrate the spectra taken with FORS2 and FORS1, respectively.

## 2.3. VLT polarimetry

Optical polarimetric observations of the afterglow were performed with VLT Antu/FORS1 and a Bessel  $R$  filter. Observations started on 2003 Feb 27.211 UT, approximately 1 day after the GRB, when the afterglow magnitude was about  $R = 20.7$ . Imaging polarimetry is achieved with a Wollaston prism splitting the image of each object in the field into the two orthogonal polarization components, which appear in adjacent areas of the CCD image. In this way, the measurement is insensitive of any variation in the source brightness during the observation. Two sets of images were acquired with four different angles (0°, 337°5, 315°0,

---

$K_s$  filters.

<sup>4</sup>The optical magnitudes of this star are  $B = 20.15 \pm 0.03$ ,  $V = 19.07 \pm 0.03$ ,  $R_c = 18.33 \pm 0.13$ ,  $I_c = 17.92 \pm 0.18$  (Henden 2003).

292<sup>s</sup>5) and with 15 min exposure each. Unfortunately, in one exposure a cosmic ray hit the afterglow, making any procedure unreliable. This set was therefore excluded from the analysis. A polarimetric standard star, Hiltner 652, was also observed in order to fix the offset between the polarization and the instrumental angles. Image reduction was performed using the *eclipse* tools (Devillard 2002), while photometry was extracted using the Gaia package<sup>5</sup>. The general procedure followed for FORS1 polarimetric observation analysis is extensively discussed, e.g., in Covino et al. (1999).

## 2.4. *Chandra* X-ray observations

A 40.17 ksec target-of-opportunity *Chandra* observation was initiated on 2003 February 27 at 16:49 UT, about 1.54 days after the GRB. Only one chip was read out (the back-illuminated S3 chip) at a frame time of 0.44 sec. Three X-ray sources are detected in the  $8 \times 8$  arcmin<sup>2</sup> field of view with a significance of more than  $5\sigma$ , two of which are within the *HETE*/*SXC* error circle. The brightest source is detected with a mean count rate of  $0.010 \pm 0.001$  cts s<sup>-1</sup>, at R.A. = 11<sup>h</sup> 33<sup>m</sup> 04<sup>s</sup>.9; Decl. = +25° 53' 55" (J2000), coincident within the error ( $\pm 0''.5$ ) with the position of the optical afterglow. This X-ray source also shows a fading by a factor of three during the observation, further strengthening its identification as the X-ray afterglow of GRB 030226. The other two sources are constant within their statistical errors, and detected at R.A. = 11<sup>h</sup> 33<sup>m</sup> 02<sup>s</sup>.8; Decl. = +25° 53' 55" and R.A. = 11<sup>h</sup> 33<sup>m</sup> 13<sup>s</sup>.9; Decl. = +25° 52' 29", respectively.

## 3. Results

### 3.1. The optical/NIR/X-ray light curve

In order to analyze the light curve of the GRB afterglow, we combined our data with published data from *Gamma-Ray Burst Coordinated Network Circulars* (GCNs<sup>6</sup>; for references see Fig. 2) and Pandey et al. (2004). In doing so, we followed the standard procedure and fitted a broken power-law decay to all photometric data. Of the available multi-wavelength data, the *R*-band light curve is sampled best. Therefore, we fitted the *R*-band light curve, using the fitting equation suggested by Beuermann et al. (1999), but in the representation

---

<sup>5</sup><http://star-www.dur.ac.uk/~pdraper/gaia/gaia.html>

<sup>6</sup>[http://gcn.gsfc.nasa.gov/gcn/gcn3\\_archive.html](http://gcn.gsfc.nasa.gov/gcn/gcn3_archive.html)

given by Rhoads & Fruchter (2001):

$$F_\nu(t) = 2^{1/n} F_\nu(t_b) [(t/t_b)^{\alpha_1 n} + (t/t_b)^{\alpha_2 n}]^{-1/n}. \quad (1)$$

Here  $F_\nu$  is the flux density<sup>7</sup>,  $\alpha_1$  and  $\alpha_2$  are the asymptotic decay indices before and after the light curve break,  $t$  is the time elapsed since the GRB trigger,  $t_b$  the break time, and  $n$  the parameter which describes the smoothness of the break. In all cases we fitted apparent magnitudes after correction for Galactic extinction. The best fit of the combined  $R$ -band data set is  $\alpha_1 = 0.50 \pm 0.35$ ,  $\alpha_2 = 2.55 \pm 0.38$ ,  $t_b = 0.83 \pm 0.10$  days, and  $n = 0.91 \pm 0.84$  ( $\chi^2/\text{d.o.f.} = 2.8$ ; Fig. 2). While similar values for  $\alpha_2$  have also been found for other afterglow light curves, the change in decay slope,  $\alpha_2 - \alpha_1$  is rather large. If we use only our  $R$ -band data (Table 2), the best fit is  $\alpha_1 = 0.70 \pm 0.25$ ,  $\alpha_2 = 2.66 \pm 0.32$ ,  $t_b = 1.04 \pm 0.12$  days, and  $n = 1.2 \pm 1.1$  ( $\chi^2/\text{d.o.f.} = 3.8$ ), consistent with the previous results. Since no evidence for an underlying host was found in our data (§ 4.1), both fits assumed a magnitude for the host of  $m = 28$  in all bands. In the following we will use the results of the first fit.

Figure 4 shows the difference between observed and best fit magnitudes, adopting for all bands the light curve parameters obtained from the  $R$ -band fit. Several small-scale fluctuations up to about 0.4 mag in both directions are apparent. In particular, on day 0.18 the optical transient is notably brighter in  $K_s$  than expected based on the light curve fit. On this day the afterglow was bright enough to do individual photometry of each NIR frame with consistent results compared to the stacked frames. This indicates that there were not any gross flattening errors since the optical transient was dithered across a fair fraction of the detector, so that some other explanation has to be invoked as to why this data point does not match the fit properly. Kulkarni et al. (2003) also noticed an unusual behavior of the afterglow light curve between 2.3 and 3.3 days after the burst. While flux fluctuations are also seen in the X-ray light curve observed with *Chandra*, a comparison of the strongest fluctuations in the  $R$  band (seen around 1.7 days after the GRB) with those in X-rays shows no obvious correlation between them (Fig. 5). However, in Fig. 5 four of the five  $R$ -band data points were taken from the literature (GCNs), so that a potential small mismatch in the photometric calibration cannot be ruled out.

### 3.2. The optical spectra

The VLT spectra of the optical transient (Figs. 6, 7) show several absorption lines, but no prominent emission lines. The latter is not surprising, as the expected lines (e.g.,

---

<sup>7</sup>We use the notation  $F_\nu \propto t^{-\alpha} \nu^{-\beta}$  for the time and frequency dependence of the flux density.

[O II] $\lambda$ 3727, [O III] $\lambda$ 5007) are located outside our wavelength band, while Ly  $\alpha$  in emission is difficult to identify. The absorption lines are due to rest-frame ultraviolet metallic lines usually present in spectra of optical afterglows and high redshift galaxies (e.g., Castro et al. 2003; Mirabal et al. 2003; Masetti et al. 2001, 2003; Savaglio et al. 2003; Shapley et al. 2003). From these lines two redshift systems at  $z=1.962\pm 0.001$  and  $z=1.986\pm 0.001$  can be determined, consistent with earlier reports (Ando et al. 2003; Chornock & Filippenko 2003; Greiner et al. 2003a; Price et al. 2003b). In addition to the therein stated absorption line systems of FeII, AlII, and CIV, we find systems of OI, CII, SiIV, and SiII. In our first epoch spectrum we also detect a feature at 5711 and 5726Å, which may be attributed to redshifted Mg II at  $z=1.042$ , a redshift system found via high-resolution spectroscopy with the Keck telescope (Chornock & Filippenko 2003; Price et al. 2003b). Based on our data we cannot identify the nature of this absorber (see also Fig. 11). Whether or not a similar feature at 5494 and 5517Å as well as 6280 and 6291Å is also due to redshifted Mg II is less certain.

Following the detection of FeII at a rest frame wavelength of 1608Å (oscillator strength  $f=0.058$ ; Prochaska et al. 2001) one would expect to see also FeII lines at rest frame wavelengths of 2344Å ( $f=0.114$ ), 2586Å ( $f=0.069$ ), 2600Å ( $f=0.239$ ) and perhaps even 2374Å ( $f=0.031$ ). Although the lines are covered by the 300V spectrum of the first night, no clear line identification can be proposed as they blend with the telluric features at observer frame wavelengths around 7000 and 7800Å (Fig. 6).

For the line fitting we used the IRAF/SPLIT task which assumes a Gaussian profile. Table 3 shows the line identifications together with the observer and rest-frame wavelengths, and the redshifts for each line detected. No line broadening and thus no velocity dispersion above the instrumental resolution is observed. In addition, the computed rest frame equivalent widths (EWs) are listed, which were calculated by dividing the measured observer frame EWs by  $(1+z)$ . Based on the measured equivalent width we calculated the column density,  $N$ , assuming the optically thin case (e.g., Spitzer 1968),

$$EW = \frac{e^2}{4\epsilon_0 m_e c^2} \lambda_{\text{rest}}^2 N f, \quad (2)$$

where the symbols  $e$ ,  $m_e$ ,  $\epsilon_0$ , and  $c$  have their usual meaning for the SI system, and  $f$  is the oscillator strength of the corresponding transition. The resulting column densities are reported in Table 3. The majority of the observed absorption lines are strong ( $EW_r > 1 \text{ \AA}$ ) and may be saturated. In that case they deviate from the linear part of the curve of growth and the approximation given in Eq. (2) has to be considered as a lower limit for the derived column densities.

Finally, the identified lines allow us to refine the redshift of the GRB to  $z=1.986$ , or

larger. Assuming a flat universe with a matter density  $\Omega_M = 0.3$ , vacuum density (cosmological constant)  $\Omega_\Lambda = 0.7$ , and Hubble constant  $H_0 = 65 \text{ km s}^{-1} \text{ Mpc}^{-1}$ , this redshift corresponds to a luminosity distance of  $5.12 \times 10^{28} \text{ cm}$  (16.6 Gpc) and a distance modulus of 46.1 mag. The look-back time is 11 Gyr. The difference in luminosity distance between both redshift systems is 245 Mpc, and the difference in velocity is  $2410 \text{ km s}^{-1}$ .

### 3.3. The spectral energy distribution of the afterglow

Of particular interest is the question whether or not the afterglow exhibited color evolution, as it has been reported for some GRBs (e.g., Bersier et al. 2003). However, given the relatively sparse data for GRB 030226 based on observing campaigns with different telescopes at different sites, we can only check for an obvious long-term trend in the color of the afterglow. Such a trend is not seen in our data (Fig. 3). Within the observational errors the break in the light curve was achromatic, and so was a potential flux variation on day 4.1 (Fig. 2). This supports the view that the break was due to a collimated explosion (Rhoads 1999; Mészáros & Rees 1999). On the other hand, around day 0.2 there is an excess flux in the  $K$  band (Fig. 4). Since the multi-color data were not taken simultaneously, we cannot decide whether this is indeed a color variation or caused by a flux variation as it has been seen in other well-studied afterglows (e.g., Lipkin et al. 2004).

Based on the above discussion we conclude that the observed spectral energy distribution (SED) of the afterglow is best described by assuming no color variations. The shape of the light curve is then the same in all photometric bands. Using the magnitude-flux conversion according to Bessel (1979) and Bessel & Brett (1988), we find that the observed mean spectral slope,  $\beta$ , across the  $BVRIJHK$  bands, corrected for Galactic extinction, is  $\beta = 0.70 \pm 0.03$  (Fig. 8), with no evidence for additional reddening by dust in the GRB host galaxy ( $A_V(\text{host})=0 \text{ mag}$ ). This holds for MilkyWay-like dust as well as for SMC-like dust, for any assumed ratio of total-to-selective extinction between  $R_V=3$  and 5. This result differs from Pandey et al. (2004) who based their conclusions exclusively on optical data obtained on days 0.62 and 1.79 after the burst ( $\beta \approx 1$ ). Pandey et al. argue that from the theoretical point of view the afterglow data are best understood if the intrinsic spectral slope was in fact  $\sim 0.55$ , requiring that the afterglow light was slightly reddened by dust in the GRB host galaxy. This spectral slope is indeed not much different from the one we deduce based on our larger data set, including NIR data, but without the need for additional reddening in the host galaxy. It is clear that the determination of  $\beta$  and the amount of reddening in a GRB host is very sensitive to the extent and quality of the data utilized.

Is there evidence for dust in the host based on the X-ray data? The *Chandra* observation

took place after the break in the light curve (for details, see Pedersen et al. 2004b). The unabsorbed X-ray flux in the 0.3–10 keV band (source frame band of 0.9–30 keV) is  $7.3 \times 10^{-14}$  erg cm $^{-2}$  s $^{-1}$ , corresponding to a mean (isotropic) luminosity of  $2.4 \times 10^{45}$  erg s $^{-1}$  (averaged over the time interval of 1.54–2.04 days after the GRB). A free power-law fit to the X-ray spectrum with just local foreground absorption yields an energy index across the 0.3 to 10 keV band of  $\beta_X = 1.04 \pm 0.20$  and a hydrogen column density  $N_H = (4 \pm 1) \times 10^{20}$  cm $^{-2}$  (Fig. 9). Since the absorbing column is above the Galactic foreground value, we performed a second fit with two different absorbing columns, namely one fixed at the Galactic value ( $N_H(\text{Gal}) = 1.8 \times 10^{20}$  cm $^{-2}$ ; Schlegel et al. 1998) and the other one at a redshift of the host galaxy of  $z = 1.986$ . The resulting energy index then is  $\beta_X = 1.08 \pm 0.15$  and the hydrogen column density in the host  $N_H(\text{host}) = (3.2 \pm 1.5) \times 10^{21}$  cm $^{-2}$ , corresponding to  $A_V(\text{host}) = 2.4$  mag (for a Galactic dust-to-gas ratio). Evidence for so much extinction in the host galaxy is definitely not seen in the optical/NIR data, a discrepancy also known from other afterglows (Galama & Wijers 2001; Hjorth et al. 2003b; Stratta et al. 2004).

Unfortunately, our VLT spectra cannot be used to derive the hydrogen column density in an independent way. The unfortunate position of Ly $\alpha$  at the short edge of our VLT spectra and the uncertainty in the spectral shape longwards of the Ly $\alpha$ -edge (Fig. 6) do not allow a quantitative treatment of the Ly $\alpha$  absorption and therefore the hydrogen column density from the optical data. On the other hand, our polarization data also exclude a large amount of dust in the GRB host galaxy along the line of sight.

### 3.4. The polarization of the afterglow

Figure 10 shows the position of the afterglow in the Stokes  $Q$ - $U$ - plane. The polarization level  $P$  is related to the Stokes parameters through  $P = \sqrt{Q^2 + U^2}$ , while the polarization angle is  $\vartheta = \frac{1}{2} \arctan(U/Q)$ . Our measurement yields for the afterglow  $Q = -0.0028 \pm 0.0030$ ,  $U = 0.0014 \pm 0.0048$  ( $1\sigma$  error), which translates, after correcting for the polarization bias (Wardle & Kronberg 1974), to a strict upper limit  $P < 1.1\%$  ( $2\sigma$ ). This is one of the lowest limits ever reported for a GRB afterglow (e.g., Covino et al. 1999, 2003b; Rol et al. 2003; Barth et al. 2003), even if values as low as  $P \approx 0.5\%$  have been measured for GRB 030329 (Greiner et al. 2003b). The low polarization of the afterglow of GRB 030226 argues against substantial dust extinction in the GRB host along the line of sight, provided that the dust properties there are not much different from those of the dust in the local universe. We conclude that the polarimetry supports the view that the average dust-to-gas ratio in the GRB host galaxy along the line of sight is much lower than those in our Galaxy.

## 4. Discussion

### 4.1. Limits on the host and a supernova component

On our VLT images and in the afterglow light curve we do not find evidence for an underlying host galaxy (Fig. 11). Spectroscopic evidence for emission lines from an underlying host is missing too (although mainly due to the insufficient wavelength coverage of our spectra). Based on our latest  $R$ -band imaging on March 13, i.e., 15 days after the burst, we conclude that  $R_{\text{host}} > 26.2$ . This estimate does not exclude the possibility that the host is indeed brighter, but some arcsec away from the burster (e.g., the objects 1 and 2 in Fig. 11), for which we have no spectroscopic confirmation.

At the given redshift of  $z=1.986$ , we do not expect to see an underlying supernova (SN) component in our data: Assuming SN 1998bw as a template (for details, see Zeh et al. 2004), this predicts an unabsorbed peak magnitude of  $R \approx 28$  approximately at day 33 and a negligible contribution to the afterglow light within the first week after the burst. That neither an underlying host galaxy nor a SN component contributes substantially to the light of the optical transient, even 1 week after the burst, means that we essentially observed an uncontaminated GRB afterglow.

### 4.2. The nature of the afterglow

An achromatic break in the light curve is generally considered as evidence for a jetted explosion (Rhoads 1999; Mészáros & Rees 1999). Using standard procedures, for the given break time and redshift as well as gamma-ray fluence the beaming corrected energy output of GRB 030226 is consistent with the ensemble statistic of bursts; the results we obtain based on our deduced break time is basically the same as in Pandey et al. (2004), and we refer the reader to this paper for a more detailed discussion on this subject.

A non-spherical explosion in the form of a highly relativistic jet should produce net polarization, and this is indeed what has been observed in a number of afterglows so far (for a review, see Covino et al. 2004). Geometrically simple models (e.g., Ghisellini & Lazzati 1999; Sari 1999) assume a uniform jet, with a constant energy per unit solid angle across the full jet. In this case, the polarization evolution has two peaks, separated by an epoch of null polarization, which roughly coincides with the break in the light curve. The polarization angle is expected to flip by  $90^\circ$  between the two peaks. More complex models (e.g., Rossi et al. 2004; Lloyd-Ronning et al. 2004) assume instead an energy distribution per solid angle which decreases towards the edge of the jet. In this case, even if the light curves are not

very different from the uniform case, the polarization is expected to show a peak close to the time of the break. Our polarization measurement of the afterglow of GRB 030226 was indeed performed very close to the break in the light curve. Interpreting this break as due to the jet effect, our low polarization value would thus favor a uniform jet over a structured jet. However, no solid conclusion can be drawn from a single upper limit, lacking monitoring of the polarization level and angle evolution with time.

An inspection of Fig. 4 shows that all photometric data concentrate around the break time, while the other part of the light curve is more poorly sampled. Depending on the extent to which we merged data taken from different groups at different optical telescopes, our results vary between strong and weak evidence for a short-term variability in the light curve. These potential short-term fluctuations, primarily at later times, are reflected in the relatively large  $1\sigma$  error bars of the deduced light curve parameters  $\alpha_1$  and  $\alpha_2$ . In particular, on day 4 after the burst, the afterglow flux is clearly below the expectations based on the light curve fit, and this holds for all optical bands (Fig. 4). Unfortunately, this is the only epoch after the break time where we have a homogeneous multi-color data set. Alternatively, there could be an excess of flux at later times ( $t > 5$  days), which cannot be attributed to an underlying host or supernova, however. In this context it is not surprising that Pandey et al. (2004) derived a different post-break decay slope of  $\alpha_2 = 2.05 \pm 0.04$  given the potential flux variations of the afterglow in combination with their much smaller monitoring time.

A key parameter of the afterglow SED is the location of the cooling frequency  $\nu_c$ , which separates fast-cooling from slow-cooling electrons (Sari et al. 1998). The combination of the *Chandra* X-ray data with the optical/NIR data places  $\nu_c$  between the X-ray and the optical bands, in agreement with the conclusion drawn by Pandey et al. (2004). Thereby the spectral slopes are similar to those found for other afterglows (e.g., GRB 010222: Masetti et al. 2001; GRB 011211: Jakobsson et al. 2003). Standard fireball models for jetted explosions with  $p > 2$  (Sari et al. 1998, 1999; Livio & Waxman 2000; Chevalier & Li 2000; Dai & Cheng 2001) then predict  $p = 2\beta + 1$  and  $\alpha_2 = p$  (i.e.,  $\alpha_2 = 2.40 \pm 0.06$  for  $\beta = 0.70 \pm 0.03$ ; § 3.3), consistent with the observed late-time decay slope of the afterglow.

Based on the above discussion we conclude that the afterglow of GRB 030226 showed all the properties already known from other bursts: an achromatic break around 1 day after the burst very likely due to a jetted outflow, a rapid decay thereafter, and possible short-term fluctuations. Finally, we can use the BOOTES-1 observations to constrain the optical emission before, during, and shortly after the genuine GRB event. A visual inspection of all BOOTES-1 frames reveals no such emission at the position of the optical afterglow, in particular simultaneously to the burst itself (Fig. 12). Therefore we derive an upper limit of  $R = 11.5$  (due to cirrus clouds present in the sky at the time of the event) for the reverse

shock emission (if any) arising from this GRB, in contrast to the 9-th magnitude prompt flash emission recorded for GRB 990123 (Akerloff et al. 1999) which demonstrates that a bright, prompt optical emission is not a generic characteristic of GRBs.

### 4.3. Clues on the GRB progenitor

Of special interest are the highly ionized absorbers Si IV and CIV and the associated absorption line systems seen in our VLT spectra separated in velocity by  $2400 \text{ km s}^{-1}$ . Schaefer et al. (2003) and Mirabal et al. (2003) discussed a similar finding for the afterglow of GRB 021004 ( $z=2.3$ ). The afterglow of this burst not only showed these lines, but four absorption line systems separated by 450, 990 and  $3155 \text{ km s}^{-1}$  (Mirabal et al. 2003; Castro-Tirado et al. 2004). Similar features were found in the afterglow of GRB 020813 (Barth et al. 2003). Schaefer et al. (2003) and Mirabal et al. (2003) have provided strong arguments that these lines, together with the observed absorption line systems, are likely to come from expanding shells around a massive Wolf-Rayet star (cf. Nugis & Lamers 2000; for a discussion, see also Wijers 2001; Chevalier et al. 2004). This could also explain the strong flux variations seen in some afterglows (e.g., GRB 000301C: Garnavich et al. 2000; Masetti et al. 2000; GRB 011211: Jakobsson et al. 2003; GRB 021004: Bersier et al. 2003; Holland et al. 2003; Lazzati et al. 2002; GRB 030329: Matheson et al. 2003), which might also be apparent for GRB 030226, even though with lower amplitude (Fig. 4). This is consistent with theoretical models that link long-duration GRBs to the explosions of massive stars (e.g., Fryer et al. 1999; Paczyński 1998; Heger et al. 2003).

For GRB 030226 the  $z=1.986$  system is clearly not a scaled version of the  $z=1.962$  system. Basically, we identify two groups of ions. Those of Si IV, Fe II, and Al II have roughly the same rest-frame equivalent widths in both redshift systems, whereas those of the other species are approximately twice as abundant in the  $z=1.986$  system compared to the  $z=1.962$  system. Within the context of the Wolf-Rayet star model this would reflect different chemical compositions of different shells in the wind, a phenomenon that is observed for example in the outer ejecta of Eta Carina (Smith & Morse 2004). While evidence for ‘line locking’ has been found in spectra taken from the afterglow of GRB 021004 (Savaglio et al. 2002; Møller et al. 2002; see also the discussion in Mirabal et al. 2003), this phenomenon is not apparent in our spectra of the afterglow of GRB 030226. If not hidden because of the medium spectral resolution, this implies that the observed features in both absorption line systems are not due to radiative acceleration of the absorbing clouds.

In principle, the presence of a strong Ly  $\alpha$  absorber in the spectrum of the afterglow of GRB 030226 implies a dense interstellar medium, possibly at the redshift of the burster.

However, in our spectra the redshift of the Ly  $\alpha$  line cannot be accurately determined. We can only place the constraint  $1.93 < z < 1.99$ . Similarly, a potential variability of the absorption lines is of interest since it could place the absorbing clouds close to the burster (e.g., Perna & Loeb 1998; Draine 2000). However, a comparison of our medium-resolution VLT spectra taken 0.2 and 1.2 days after the burst does not reveal evidence for a general variation in the line strengths. Unfortunately, the Ly  $\alpha$  line is difficult to analyze in this respect given its unfavorable position at the very blue side in our VLT spectra.

While our spectral data support the view that the GRB progenitor was a massive star, there is no evidence for a stellar wind profile in the light curve data, similar to other cases (cf. Chevalier & Li 2000; Panaitescu & Kumar 2002). Within the framework of standard afterglow models with  $p > 2$  the light curve parameter  $\alpha_1$  is related to the density profile of the circumburst medium,  $n(r) \sim r^{-k}$ , by  $\alpha_1 = 3/4(p-1) + k/(8-2k)$  (e.g., Mészáros, Rees, & Wijers 1998; Dai & Wu 2003). In the ideal case  $k = 0$  means an ISM-shaped interstellar medium, while  $k = 2$  refers to a stellar wind. Using  $\alpha_1 = 0.50 \pm 0.35$  and  $p > 2$  a density profile with  $k=2$  is basically ruled out. Also the rather steep change in the decay slope between 0.5 and 2 days after the burst from  $\alpha_1 = 0.50 \pm 0.35$  to  $\alpha_2 = 2.55 \pm 0.38$  might be difficult to explain with a standard wind profile. But does this really argue against WR stars as GRB progenitors? There is increasing observational evidence that the outer winds of these stars might indeed be very clumpy (e.g., Crowther et al. 2002) with the wind properties depending on the viewing direction, comparable to the one of Eta Carina (see Fig. 1 in van Boekel et al. 2003; Smith et al. 2003). An ansatz with  $k = 2$  to describe the stellar wind might then be an oversimplification; in reality  $k$  might be notably smaller (Wijers 2001). More insight on the properties of winds from WR stars and more spectroscopic afterglow data are required in order to tackle this problem. A monitoring of the evolution of the cooling frequency across the optical/NIR bands in GRB afterglows, which might become possible in the *Swift* era (Gehrels 2004), might also help to clarify this issue.

## 5. Summary

We have presented a comprehensive data set of the afterglow of GRB 030226, consisting of optical, NIR, and X-ray observations, including VLT spectroscopy and VLT polarimetry. Concerning the nature of the GRB afterglow our basic findings are the following:

1. The evolution of the afterglow was achromatic within the observational errors over the optical/NIR bands analogous to other bursts (e.g., GRB 000301C: Jensen et al. 2001; GRB 020405: Masetti et al. 2003). A break in the light curve occurred  $\sim 1$  day after the burst. The break was rather smooth, similar to that found for, e.g., GRB 990510

(Harrison et al. 1999).

2. Because the break was achromatic we interpret it as due to a jetted explosion. Close to the break time the intrinsic linear polarization of the afterglow was very low ( $< 1.1\%$ ), which favors a uniform jet over a structured jet.
3. After correction for Galactic extinction, the best fit multi-color lightcurve has a spectral slope across the optical/NIR bands of  $\beta = 0.70 \pm 0.03$ , with no sign of additional reddening due to dust in the host galaxy. This is in contrast to the *Chandra* X-ray data, which point to a relatively large hydrogen column density along the line of sight. This perhaps indicates a reduced dust-to-gas ratio in the GRB environment, similar to suggestions made for several other GRB afterglows (Galama & Wijers 2001; Hjorth et al. 2003b; Stratta et al. 2004).
4. In the 0.3–10 keV region the spectral slope was  $\beta = 1.04 \pm 0.20$  on day 1.6–2, which together with the spectral slope across the optical/NIR bands places the cooling frequency between the optical bands and the X-ray region.

In addition, based on BOOTES-1 observations no prompt optical flash coincident with the gamma-ray burst was detected. We place an upper limit of  $R = 11.5$  on the reverse shock emission arising from this burst.

While our multi-wavelength observations trace the evolution of the afterglow, our VLT spectroscopy provides insight on the nature of the GRB environment, even though an underlying host galaxy remained undetected down to a faint flux level ( $R > 26.2$ ). In particular, beside a foreground absorber at  $z=1.042$  we found two absorption line systems at redshifts  $z=1.962$  and  $z=1.986$ , with the higher value as a lower limit for the redshift of the burster. Both line systems reveal an interstellar gas composed of highly ionized species (Si IV, C IV). This, together with the inferred separation in velocity of  $2400 \text{ km s}^{-1}$  between both systems, is very similar to observations of the afterglow of GRB 021004 (Castro-Tirado et al. 2004; Schaefer et al. 2003; Mirabal et al. 2003), and possibly indicative of a fast stellar wind placed in a strong radiation field. Within this context the data support an association of GRBs with Wolf-Rayet stars. They also call for early spectroscopy of as many GRB afterglows as possible in order to search for potential line features from stellar winds. It is surely premature to claim that all GRB progenitors are associated with WR stars, but among all progenitor models discussed so far in the literature (cf. Fryer et al. 1999) they are most promising from a theoretical point of view, and significantly supported by present-day observations.

## 6. Acknowledgments

We are indebted to the ESO staff at La Silla and at Paranal, in particular Malvina Billeres, Lisa Germany, Swetlana Hubrig, Nuria Huélamo, Norma Hurtado, Elena Mason, Leonardo Vanzi for prompt execution of the observing requests and additional efforts related to that. We also thank H. Navasardyan for the coordination and execution of the Asiago observations in Service Mode. J.G. and K.P. are particularly grateful to H. Tananbaum for granting the *Chandra* observing time. S.K. acknowledges support from the Deutsche Akademische Austauschdienst (DAAD) under grants No. D/0237747 and D/0103745 and from the Deutsche Forschungsgemeinschaft (DFG) under grant Kl766/11. N.M., both E.P., and E.M. acknowledge support under CRUI Vigoni program 31-2002. D.H.H. acknowledges support under NSF grant INT-0128882. A.Z. acknowledges financial support from the Friedrich-Schiller-University, Jena, Germany, and from the DFG under grant Kl766/11. K.P. acknowledges support from the Carlsberg foundation. A.J.C.-T. acknowledges support from INTA and the Spanish Programme AYA 2004-01515 as well as the encouraging work of T. J. Mateo Sanguino, P. Kubánek and S. Vitek. This research has made use of the NASA/IPAC Infrared Science Archive, which is operated by the Jet Propulsion Laboratory, California Institute of Technology, under contract with the National Aeronautics and Space Administration. We thank the anonymous referee for valuable comments.

### A. AB offsets

Table 1: Conversion constants for the transformation into the AB magnitude system (Oke & Gunn 1983).<sup>a</sup>

Instrument	Filter	eff. wavelength	AB <sub>off</sub>
VLT/FORS1	<i>B</i> _Bess +34	429 nm	−0.10
VLT/FORS1	<i>V</i> _Bess +35	554 nm	0.03
VLT/FORS1	<i>R</i> _Bess +36	657 nm	0.23
VLT/FORS1	<i>I</i> _Bess +37	768 nm	0.44
VLT/FORS2	<i>V</i> _Bess +75	554 nm	0.06
VLT/ISAAC	<i>J<sub>s</sub></i>	1240 nm	0.90
VLT/ISAAC	<i>H</i>	1650 nm	1.38
VLT/ISAAC	<i>K<sub>s</sub></i>	2160 nm	1.86
NTT/EMMI	<i>B</i> #605	413.9 nm	−0.16
NTT/EMMI	<i>V</i> #606	542.6 nm	0.02
NTT/EMMI	<i>R</i> #608	641.0 nm	0.22
NTT/SuSI2	Bessel <i>B</i> #811	421.2 nm	−0.06
NTT/SuSI2	Bessel <i>R</i> #813	641.6 nm	0.21
NOT/ALFOSC	<i>U</i> #7	362 nm	0.72
NOT/ALFOSC	<i>V</i> #75	530 nm	0.01
TNG/Dolores	<i>U</i> #01	361 nm	0.78

<sup>a</sup>For the VLT/ISAAC filters the AB offset [mag] was taken from Labbé et al. (2003) and Gorosabel et al. (2003). For the other cases AB offsets were calculated in the present work using the effective wavelengths and detector quantum efficiencies as provided at the webpages of the corresponding observing sites.

## REFERENCES

- Akerloff, C., Balsano, R., Barthelmy, S., et al. 1999, *Nat.*, 398, 400
- Ando, M., Ohta, K., Watanabe, C., et al. 2003, *GCN Circ.* 1884
- Barth, A. J., Sari, R., Cohen, M. H., et al., 2003, *ApJ*, 584, L47
- Bersier, D. et al. 2003, *ApJ*, 584, L43
- Bessel, M. S. 1979, *PASP*, 91, 589
- Bessel, M. S., & Brett, J. M. 1988, *PASP*, 100, 1134
- Beuermann, K., Hessman, F. V., Reinsch, K., et al. 1999, *A&A* 352, L26
- Castro, S., Galama, T. J., Harrison, F. A., et al. 2003, *ApJ*, 586, 128
- Castro-Tirado, A. J., Soldán, J., Rezek, T., et al. 1999, *A&AS*, 138, 583
- Castro-Tirado, A. J., de Ugarte Postigo, A., Mateo, T. J., et al. 2003, *GCN Circ.* 1887
- Castro-Tirado, A. J., et al. 2004, in preparation
- Chevalier, R. A., Li, Z.-Y, 2000, *ApJ*, 536, 195
- Chevalier, R. A., Li, Z.-Y, & Fransson, C. 2004, *ApJ*, 606, 369
- Chornock, R., & Filippenko, A. V. 2003, *GCN Circ.* 1897
- Covino, S., Lazzati, D., Ghisellini, G., et al., 1999, *A&A*, 348, L1
- Covino, S., Ghisellini, G., Lazzati, D., & Malesani, D., 2004, in *ASP Conf. Ser. "Gamma Ray Bursts in the Afterglow Era — Third Workshop"*, ed. L. Piro and M. Feroci (preprint: astro-ph/0301608)
- Covino, S., Ghisellini, G., Malesani, D., et al. 2003a, *GCN Circ.* 1909
- Covino, S., Malesani, D., Tavecchio, F., et al. 2003b, *A&A*, 404, L5
- Crowther, P. A., Dessart, L., Hillier, D. J., Abbott, J. B., Fullerton, A. W. 2002, *A&A*, 392, 653
- Dai, Z. G., & Cheng, K. S. 2001, *ApJ*, 558, L109
- Dai, Z. G., & Wu, X. F. 2003, *ApJ*, 591, L21
- Devillard, N. 2002, *Eclipse Users Guide*, at URL  
[www.eso.org/projects/aot/eclipse/eug/eug/eug.html](http://www.eso.org/projects/aot/eclipse/eug/eug/eug.html)
- Draine, B. T. 2000, *ApJ*, 532, 273
- Fatkhullin, T., Komarova, V., Sokolov, V., et al. 2003, *GCN Circ.* 1925
- Fox, D. W., Chen, H. W., & Price, P. A. 2003, *GCN Circ.* 1879

- Fox, D. W., et al. 2004, in: Proc. GRB 2003 conference, Santa Fe
- Fryer, C. L., Woosley, S. E., & Hartmann, D. H. 1999, ApJ, 526, 152
- Galama, T. J., & Wijers, R. A. M. J. 2001, ApJ, 549, L209
- Garnavich, P. M., Loeb, A., Stanek, K. Z. 2000, ApJ, 544, L11
- Garnavich, P. M., von Braun K., & Stanek, K.Z. 2003, GCN Circ. 1885
- Gehrels, N. 2004, New Astron. Reviews, 48, 431
- Ghisellini, G., & Lazzati, D., 1999, MNRAS, 309, L7
- Gorosabel, J., Klose, S., Christensen, L., Fynbo, J. P. U., Hjorth, J., et al. 2003, A&A, 400, 127
- Greiner, J., Guenther, E., Klose, S., & Schwarz, R. 2003a, GCN Circ. 1886
- Greiner, J., Klose, S., Reinsch, K., et al. 2003b, Nature, 426, 157
- Guarnieri, A., et al. 2003, GCN Circ. 1892
- Harrison, F. A., Bloom, J. S., Frail, D. A., et al. 1999, ApJ, 523, L121
- Hawarden, T. G., Leggett, S. K., Letawsky, M. B., et al. 2001, MNRAS, 325, 563
- Heger, A., Fryer, C. L., Woosley, S. E., et al. 2003, ApJ, 591, 288
- Henden, A. A. 2003, GCN Circ. 1916
- Hjorth, J., Sollerman, J., Møller, P., et al. 2003a, Nature, 423, 847
- Hjorth, J., Møller, P., Gorosabel, J., et al. 2003b, ApJ, 597, 699
- Holland, S. T., Weidinger, M., Fynbo, J. P. U., et al. 2003, AJ, 125, 2291
- Jakobsson, P., Hjorth, J., Fynbo, J. P. U., et al. 2003, A&A, 408, 941
- Jensen, B. L., Fynbo, J. P. U., Gorosabel, J., et al. 2001, A&A, 370, 909
- Kawabata, K. S., Deng, J., Wang, L., et al. 2003, ApJ, 593, L19
- Kulkarni, S. R., Fox, D. W., Berger, E., et al. 2003, GCN Circ. 1911
- Labbé, I., Franx, M., Rudnick, G., et al. 2003, AJ, 125, 1107
- Lazzati, D., Rossi, E., Covino, S., Ghisellini, G., & Malesani, D. 2002, A&A, 396, L5
- Lipkin, Y. M., Ofek, E. O., Gal-Yam, A., Leibowitz, E. M., Poznanski, D., et al. 2004, ApJ, 606, 381
- Livio, M., & Waxman, E. 2000, ApJ, 538, 187
- Lloyd-Ronning, N., Dai, X., & Zhang, B., 2004, ApJ, 601, 371
- Malesani, D., Tagliaferri, G., Chincarini, G., et al. 2004, ApJ, 609, L5

- Masetti, N., Bartolini, C., Bernabei, S., et al. 2000, *A&A*, 359, L23
- Masetti, N., Palazzi, E., Pian, E., et al. 2001, *A&A*, 374, 382
- Masetti, N., Palazzi, E., Pian, E., et al. 2003, *A&A*, 404, 465
- Matheson, T., Garnavich, P. M., Stanek, K., et al. 2003, *ApJ*, 599, 394
- Mészáros, P., & Rees, M. 1999, *MNRAS*, 306, L39
- Mészáros, P., Rees, M., & Wijers, R. A. M. J. 1998, *ApJ*, 499, 301
- Mirabal, N., Halpern, J. P., Chornock, R., et al. 2003, *ApJ*, 595, 935
- Møller, P., Fynbo, J.P.U., Hjorth, J., et al. 2002, *A&A*, 396, L21
- Nugis, T., & Lamers, H. J. G. L. M. 2000, *A&A*, 360, 227
- Oke, J. B., & Gunn, J. E. 1983, *ApJ*, 266, 713
- Paczynski, B. 1998, *ApJ*, 494, L45
- Panaitescu, A., & Kumar, P. 2002, *ApJ*, 571, 779
- Pandey, S. B., Sagar, R., Anupama, G. C., et al. 2004, *A&A*, 417, 919
- Pedersen, K., Fynbo, J., Hjorth, J., Watson, D., et al. 2004a, *GCN Circ.* 1924
- Pedersen, K., et al. 2004b, in preparation
- Perna, R., & Loeb, A. 1998, *ApJ*, 501, 467
- Persson, S. E., Murphy, D. C., Krzeminski, W., et al. 1998, *AJ*, 116, 2475
- Price, P. A., Fox, D.W., & Chen, H.W. 2003a, *GCN Circ.* 1880
- Price, P. A., Fox, D.W., Djorjovski, S. G., et al. 2003b, *GCN Circ.* 1889
- Price, P. A. & Warren, B. E. 2003, *GCN Circ.* 1890
- Prochaska, J. X., Wolfe, A. M., Tytler, D., et al. 2001, *ApJS*, 137, 21
- Rhoads, J. E. 1999, *ApJ*, 525, 737
- Rhoads, J. E. & Fruchter A. S., 2001, *ApJ*, 546, 117
- Rol, E., Wijers, R. A. M. J., Fynbo, J. P. U., et al., 2003, *A&A*, 405, L23
- Rossi, E. M., Lazzati, D., Salmonson, J. D., & Ghisellini, G., 2004, *MNRAS*, submitted
- Rumyantsev, V., Biryukov, V., & Pozanenko, A. 2003a, *GCN Circ.* 1908
- Rumyantsev, V., Biryukov, V., & Pozanenko, A. 2003b, *GCN Circ.* 1929
- Sari, R. 1999, *ApJ*, 524, L43
- Sari, R., Piran, T. & Narayan, R. 1998, *ApJ*, 497, L17

- Sari, R., Piran, T. & Halpern, J.P. 1999, *ApJ*, 519, L17
- Savaglio, S., Fiore, F., Israel, G., et al. 2002, *GCN Circ.* 1633
- Savaglio, S., Fall, S. M. & Fiore, F. 2003, *ApJ*, 585, 638
- Schaefer, B. E., Gerardy, C. L., Höflich, P., et al. 2003, *ApJ*, 588, 387
- Schlegel, D., Finkbeiner, D., & Davis, M. 1998, *ApJ*, 500, 525
- Shapley, A. E., Steidel, C., Pettini, M., & Adelberger, K. L. 2003, *ApJ*, 588, 65
- Semkov, E. 2003, *GCN Circ.* 1935
- Smith, N., Davidson, K., Gull, T. R., Ishibashi, K., & Hillier, D. J. 2003, *ApJ*, 586, 432
- Smith, N., & Morse, J. A. 2004, *ApJ*, 605, 854
- Spitzer, L. 1968, *Diffuse Matter in Space* (New York: Wiley), 19
- Stanek, K. Z., Matheson, T., Garnavich, P. M., et al. 2003, *ApJ*, 591, L17
- Stratta, G., Fiore, F., Antonelli, L. A., Piro, L., de Pasquale, M. 2004, *ApJ*, 608, 846
- Suzuki, M., Shirasaki, Y., Graziani, C., et al. 2003, *GCN Circ.* 1888
- van Boekel, R., et al. 2003, *A&A*, 410, L37
- von Braun, K., Garnavich, P., & Stanek, K. 2003, *GCN Circ.* 1902
- Vreeswijk, P. M., Ellison, S. L., Ledoux, C., et al. 2004, *A&A*, 419, 927
- Wardle, J. F. C., & Kronberg, P. P., 1974, *ApJ*, 194, 249
- Wijers, R. A. M. J. 2001, in *Second Rome Workshop on GRBs in the Afterglow Era*, E. Costa, F. Frontera, & J. Hjorth (Berlin: Springer), 306
- Zeh, A., Klose, S., & Hartmann, D. H. 2004, *ApJ*, 609, 952

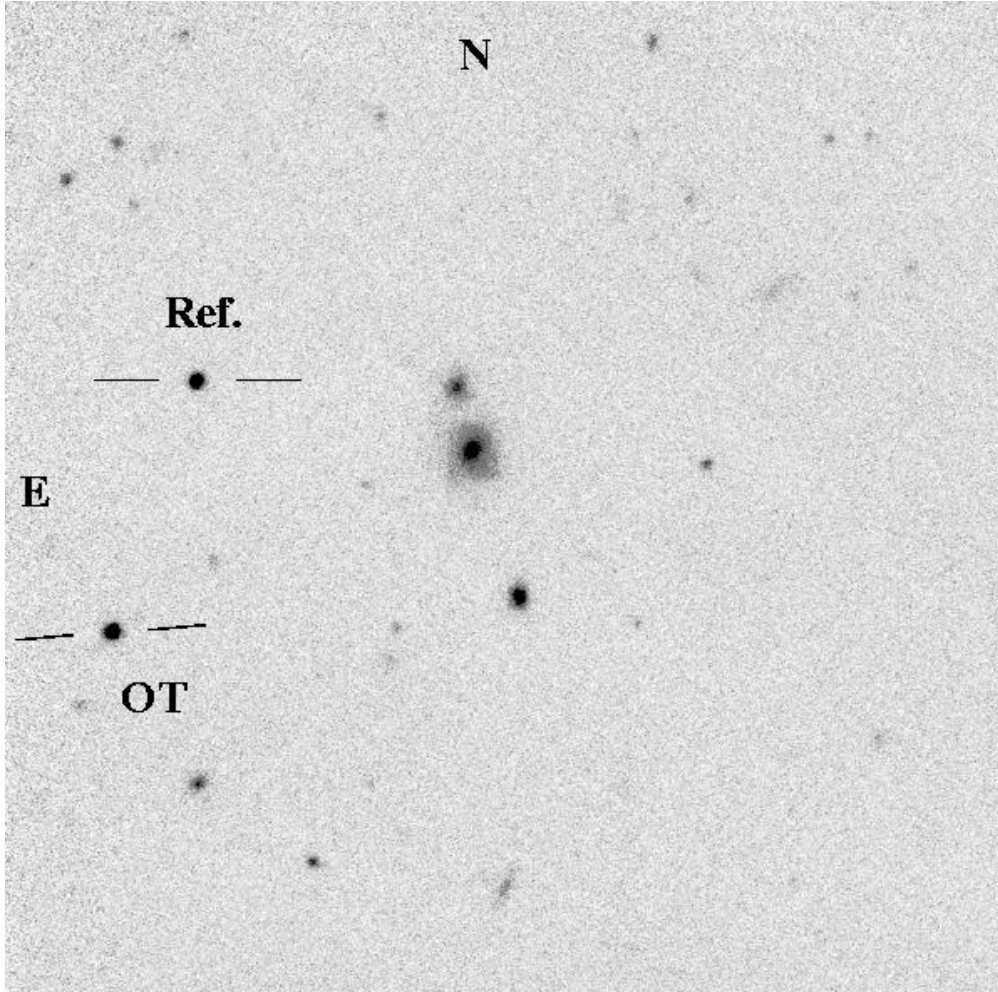


Fig. 1.— VLT/ISAAC  $K_s$ -band images of the afterglow of GRB 030226 obtained 4.5 hrs after the burst. The image size is approximately  $100'' \times 100''$ ; ‘Ref’ denotes the reference star, which we used for the NIR photometry (see § 2.1).

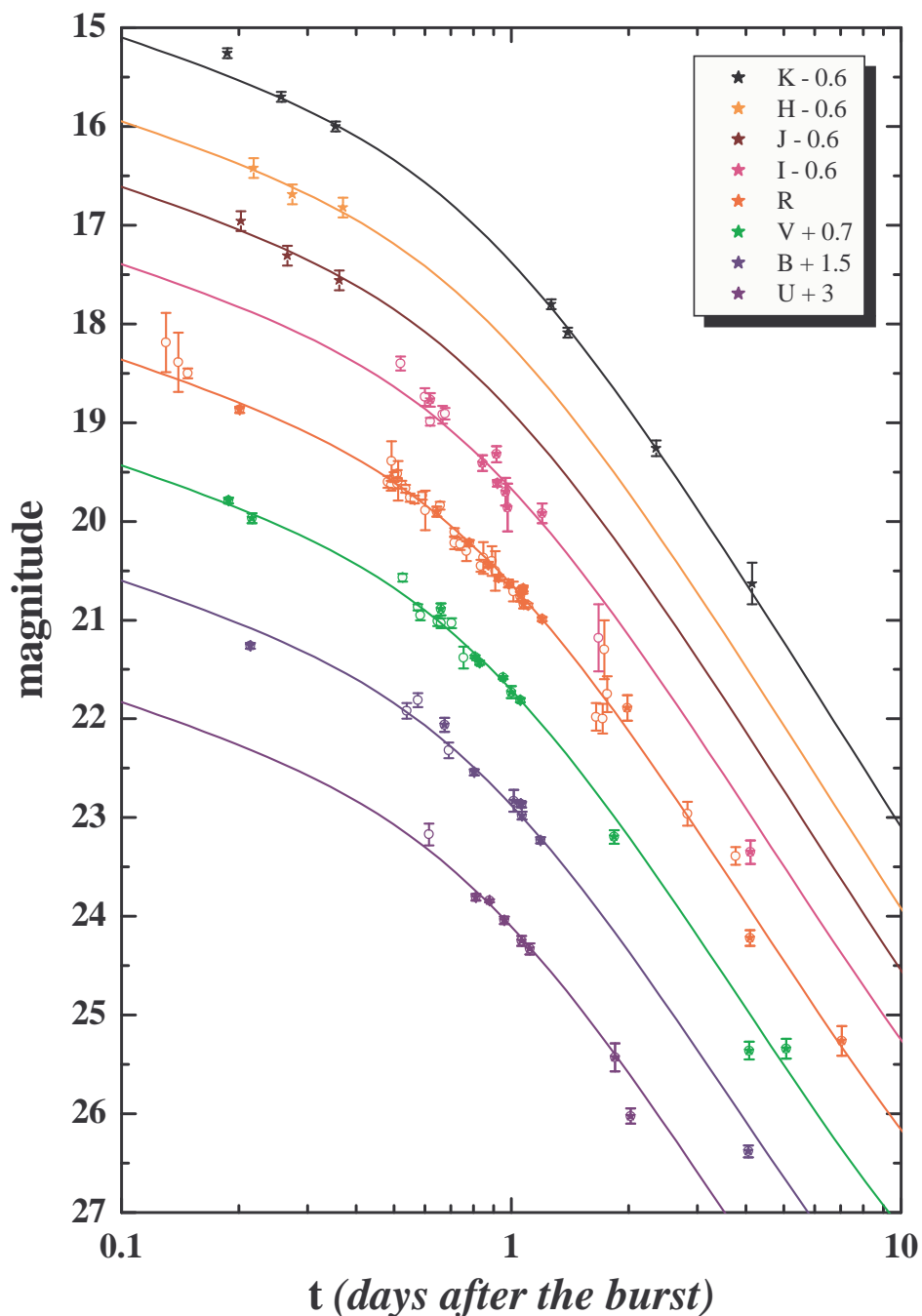


Fig. 2.— Multi-color light curve of the optical transient following GRB 030226. Data from Table 2 are shown here (stars) together with data (open circles) reported in various Gamma-Ray Burst Circulares (Ando et al. 2003; Garnavich et al. 2003; Price & Warren 2003; Guarnieri et al. 2003; von Braun et al. 2003; Rumyantsev et al. 2003a,b; Covino et al. 2003a; Fatkhullin et al. 2003; Semkov 2003) and by Pandey et al. (2004). Note that the  $R$ -band data reported in GCNs # 1881, 1882, 1884, 1890, and 1908 were corrected for a 0.4 mag offset at the zero point.

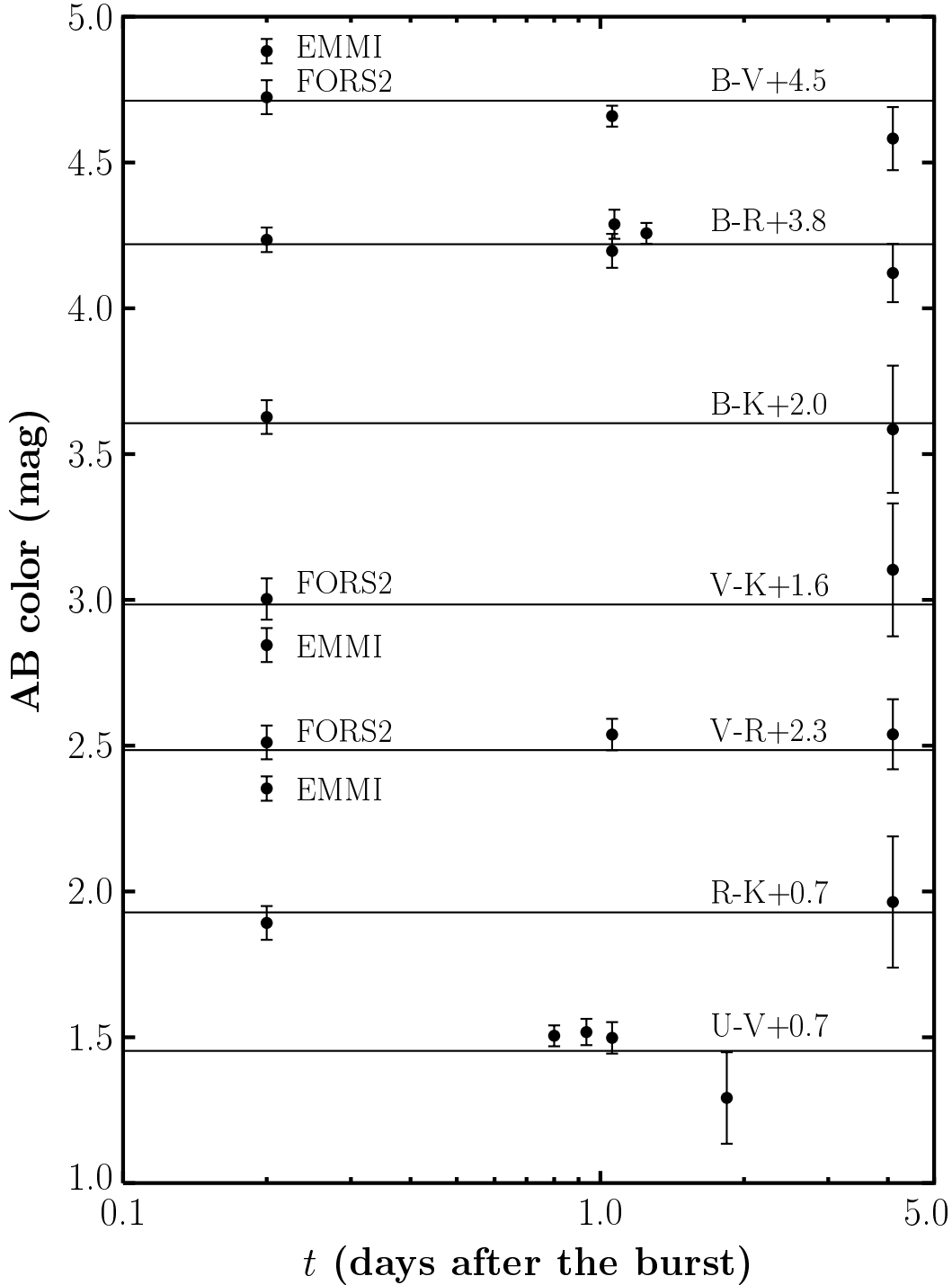


Fig. 3.— The color of the afterglow as a function of time, not corrected for Galactic extinction. The color was calculated from AB magnitudes, with the AB offsets given in Table 1. Only data from telescopes with known AB offsets were used. Straight lines give the mean of the corresponding color. Even though we cannot resolve the origin for the offset between the NTT/EMMI and VLT/FORS2  $V$ -band data during the first observing epoch, we favor the view that our data (Table 2) point to an achromatic evolution of the afterglow between 0.2 and 4 days after the burst.

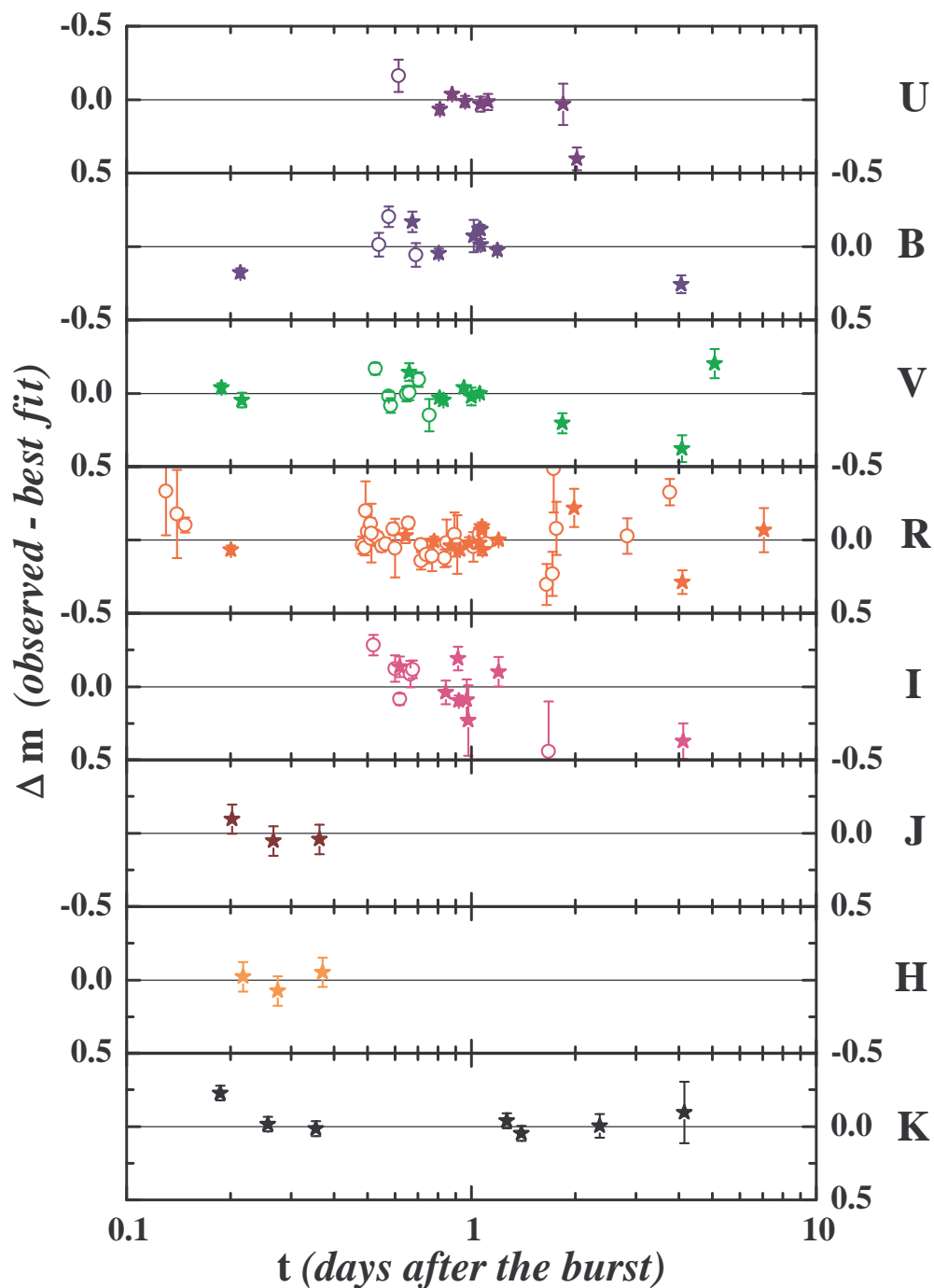


Fig. 4.— Observed minus best fit magnitudes (based on the  $R$ -band fit; Fig. 2) for the data from Table 2 together with data reported in several GCNs (for references, see Fig. 2) and by Pandey et al. (2004). The scale at the left ordinate refers to  $U, V, I, H$ , the right to  $B, R, J, K$ .  $\Delta m < 0$  means an excess of flux with respect to the fit. Symbols follow Fig. 2.

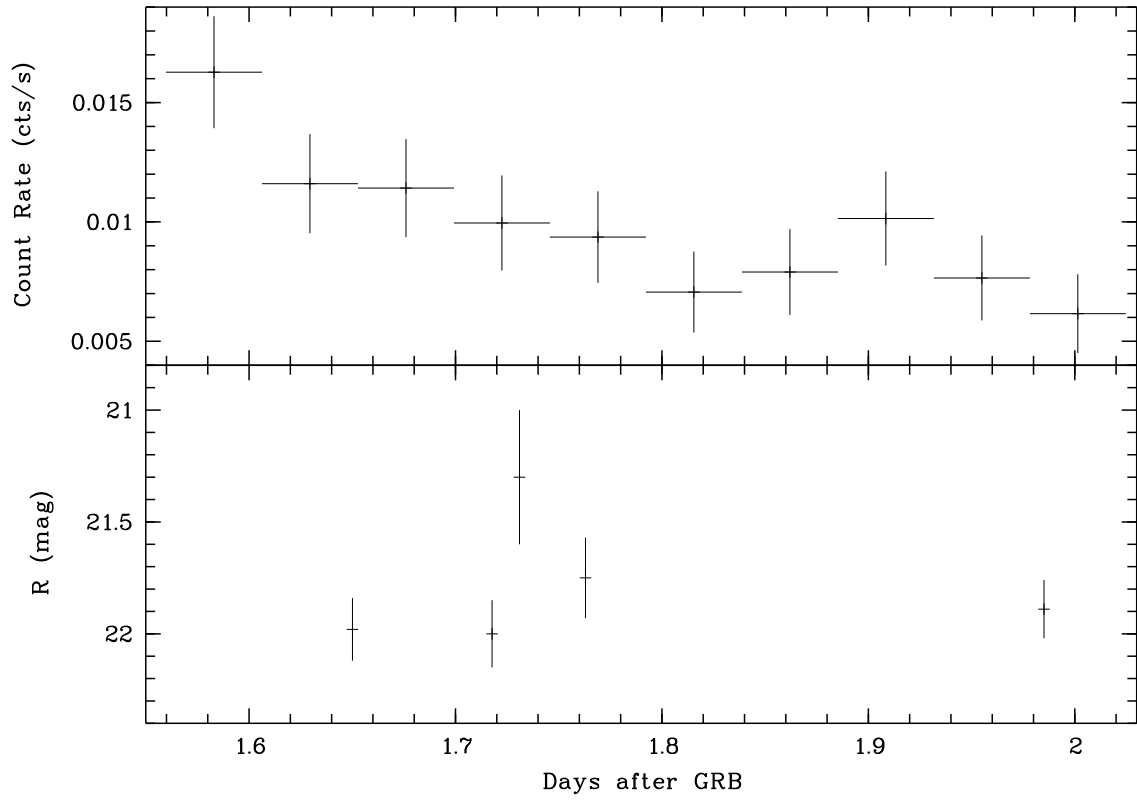


Fig. 5.— X-ray light curve obtained with *Chandra* (top panel) and the contemporaneous optical observations (bottom panel) from Fatkhullin et al. (2003), Semkov (2003), Pandey et al. (2004), and our observing run (Table 2).

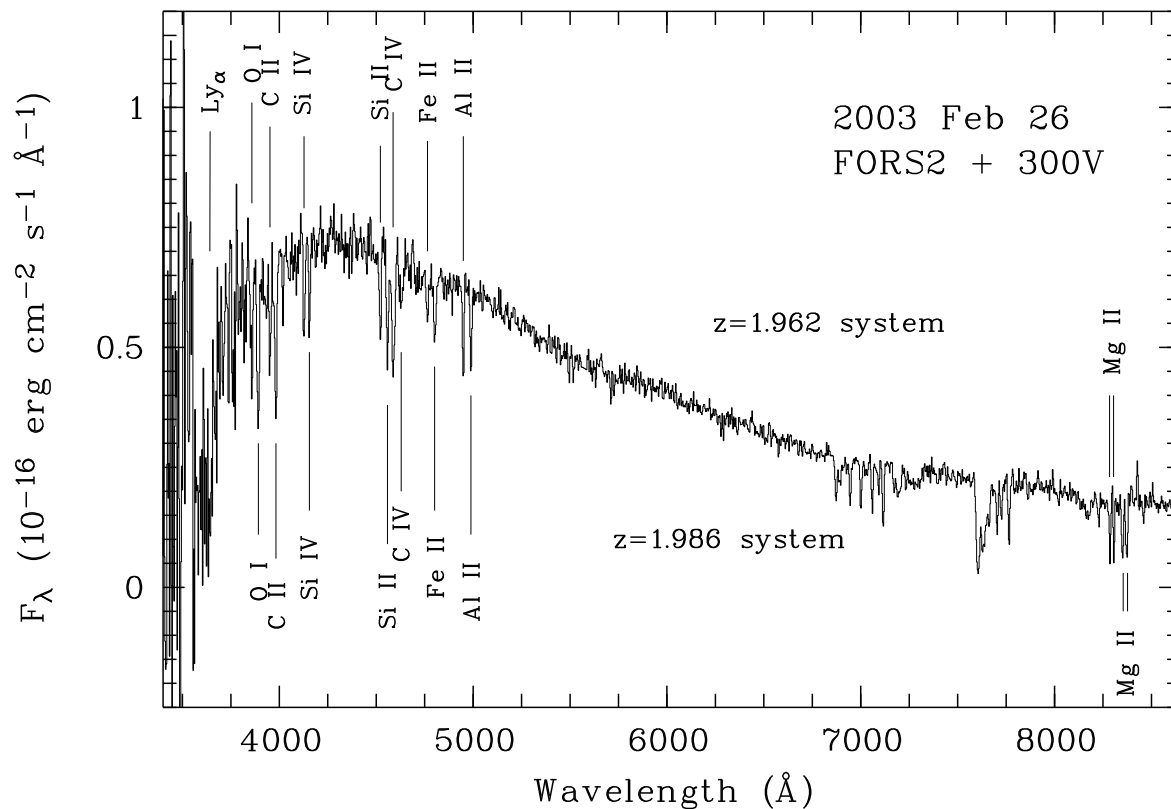


Fig. 6.— Short-wavelength part of the VLT/FORS2 spectrum using the 300V grism taken on 2003 February 26, five hours after the burst. Two distinct redshift systems at  $z=1.962$  and  $z=1.986$  are detected. Line identifications are indicated. Note the broad Ly  $\alpha$  absorption feature. Some telluric lines between  $\sim 6500$  and  $8000 \text{ \AA}$  could not be removed during the calibration process. Also, the rather unexpected curvature in the blue wavelength range is probably unreal and may be a residual of the flux calibration.

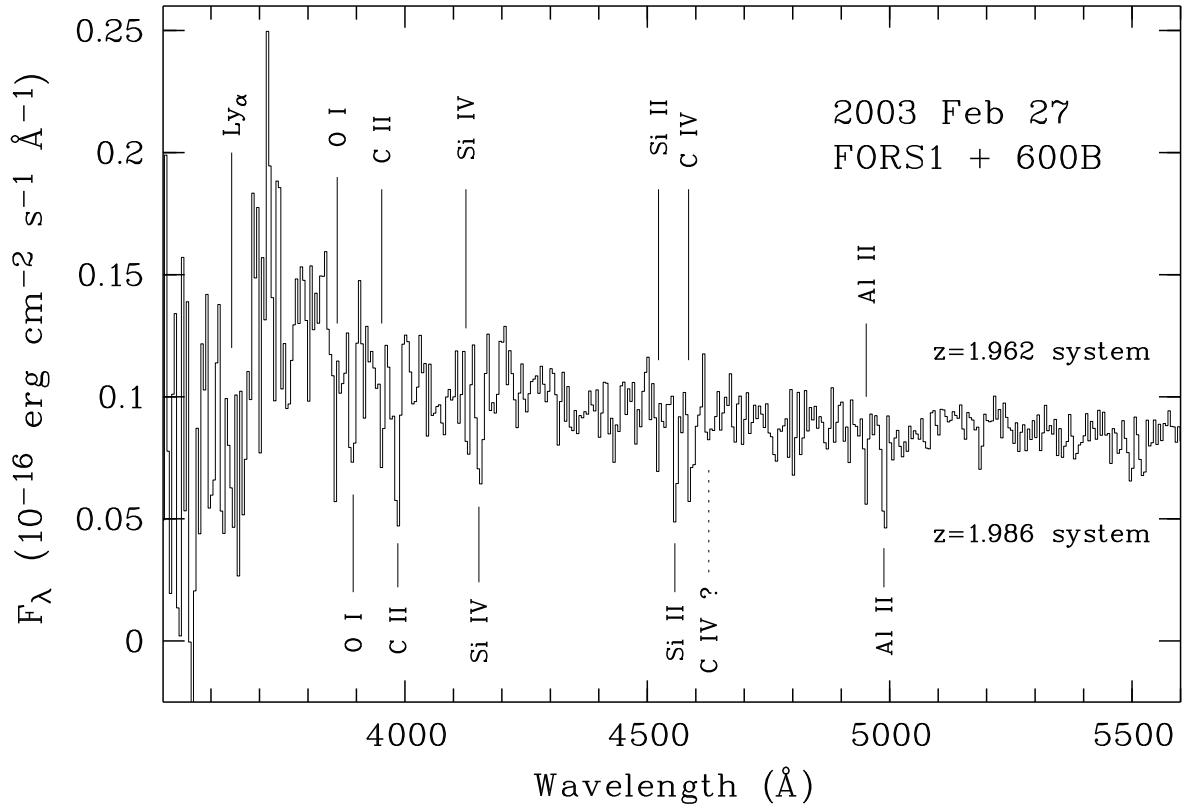


Fig. 7.— VLT/FORS1 spectrum from the GRB afterglow using the 600B grism taken on 2003 February 27, twenty nine hours after the burst and thus shortly after the break in the light curve.

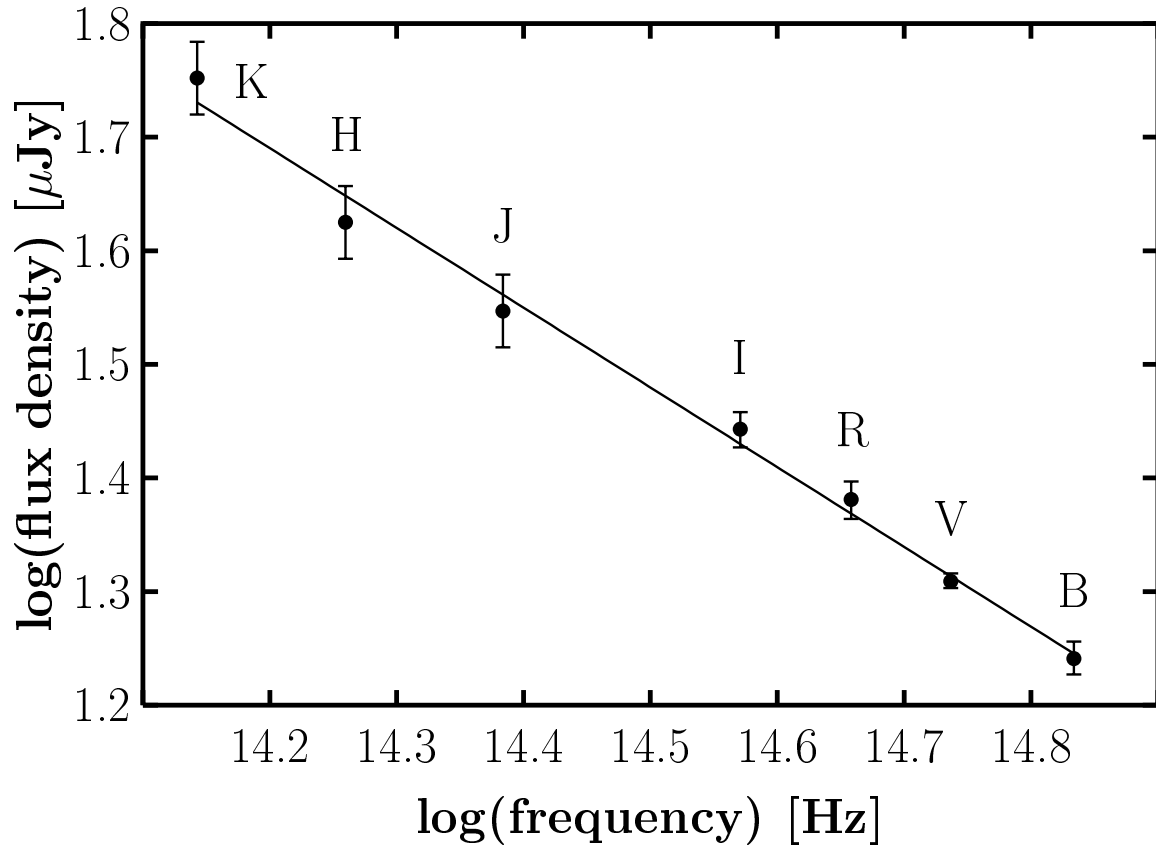


Fig. 8.— Spectral energy distribution of the afterglow at the time of the light curve break ( $t_b$ ; § 3.1). The data are corrected for Galactic extinction.

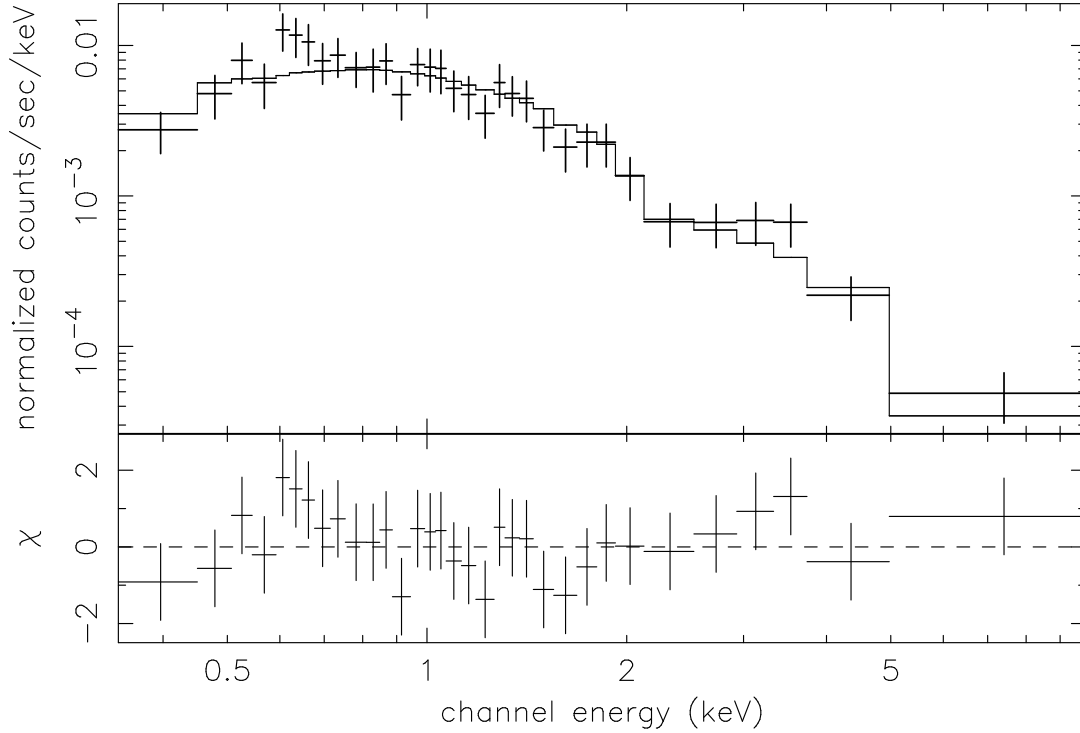


Fig. 9.— The X-ray count spectrum (top) of the GRB 030226 afterglow, integrated over the full observation time (1.54–2.04 days after the GRB). A power-law model (full line) gives a reasonably accurate fit ( $\chi^2/\text{d.o.f.}=0.7$ ; deviations from the power law fit in units of  $\sigma$  are shown in the bottom panel) with a spectral slope  $\beta_X = 1.04 \pm 0.20$ .

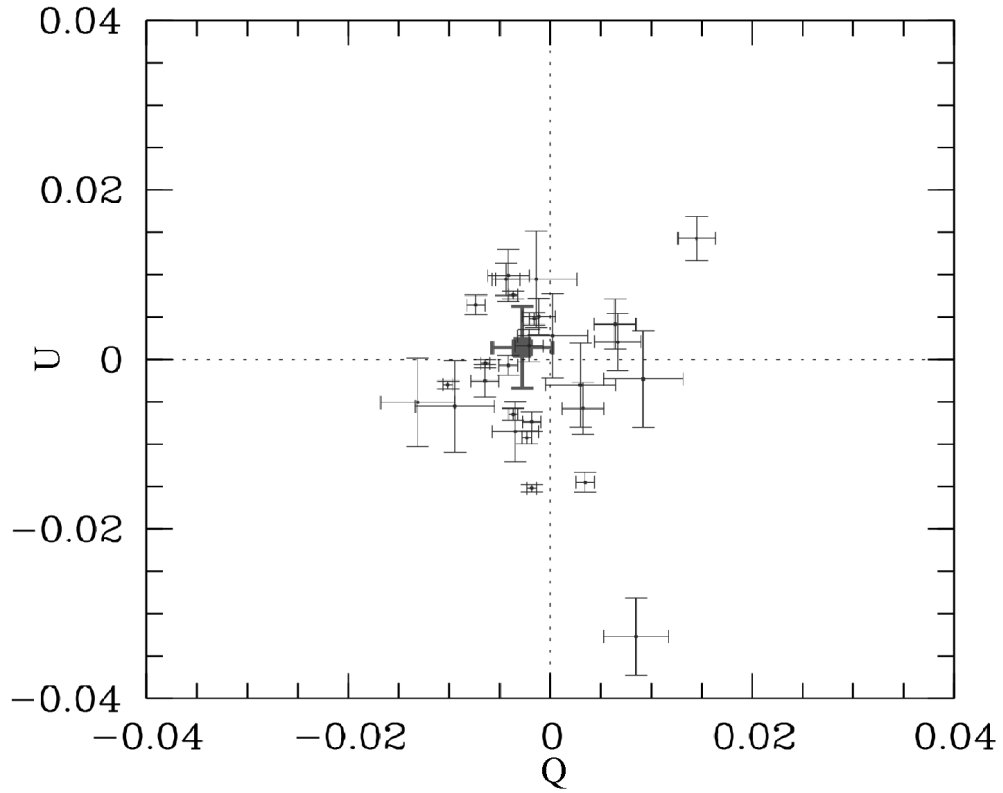


Fig. 10.— Stokes  $Q$ - $U$ -plane showing the position of the afterglow (big dot) compared with that of field stars. The average polarization of field stars is also close to zero, as it is expected towards such a low-reddening line of sight.

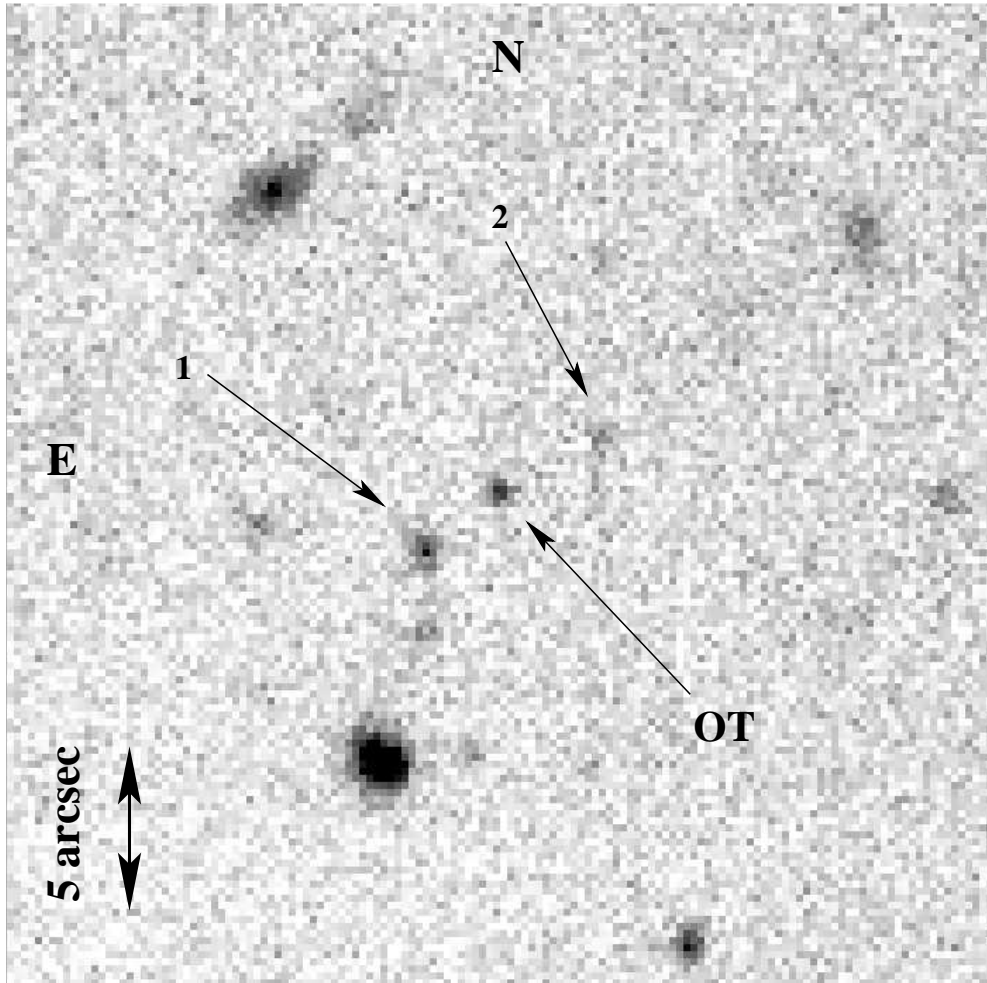


Fig. 11.— VLT/FORS1 *R*-band image taken on March 2, four days after the burst. At that time the magnitude of the optical afterglow was  $R=24.2$ . There are two sources within  $2''.5$  radius around the optical transient (indicated by numbers and arrows). Without having spectral data at hand, we cannot exclude that one of them is the host. However, in such a case the GRB would have occurred at a rather large projected distance from the luminosity center of the host: At  $z=1.986$  an angular distance of  $1''$  corresponds to 9 kpc. It is conceivable that one of these sources is responsible for the foreground absorber of Mg II at  $z=1.042$  we found in our spectra (§ 3.2).

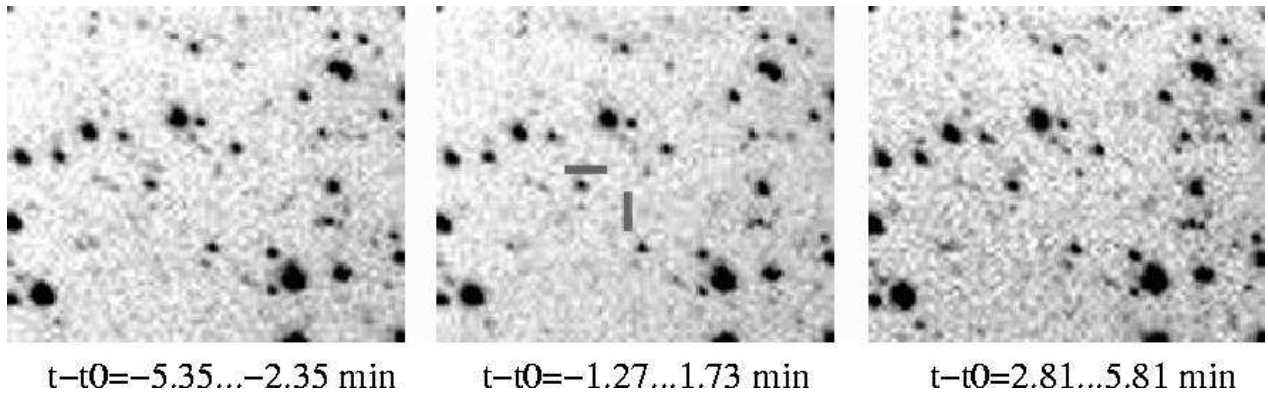


Fig. 12.— Unfiltered exposures (180-s each) obtained by the BOOTES-1 wide field camera covering the GRB 030226 error box. The images covered the period 03:41 - 03:52 UT on 26 Feb 2003 (i.e., between 5.3 min before the trigger and 5.8 min after the trigger). The ticks mark the position of the optical afterglow. The depicted field is  $2 \times 2$  deg<sup>2</sup>. Note that there is some degree of geometrical distortion due to the fact that the images were taken with a wide-field optical system. North is up and east to the left.

Table 2. Log of the observations

Date (UT)	$\langle dt \rangle$ (days) <sup>a</sup>	Tel./Instr.	Filter/Grism	Exp. (s)	magnitude
2003 Feb 26, 08:04	0.1868	VLT/ISAAC	$K_s$	15×10	15.95±0.05
2003 Feb 26, 08:09	0.1882	NTT/EMMI	$V$	3×300	19.09±0.03
2003 Feb 26, 08:27	0.2007	NTT/EMMI	$R$	3×300	18.87±0.03
2003 Feb 26, 08:29	0.2024	VLT/ISAAC	$J_s$	10×30	17.56±0.10
2003 Feb 26, 08:43	0.2062	VLT/FORS2	$V$	1×10	19.27±0.05
2003 Feb 26, 08:46	0.2139	NTT/EMMI	$B$	3×300	19.76±0.03
2003 Feb 26, 08:52	0.2173	VLT/FORS2	300V	1×900	...
2003 Feb 26, 08:49	0.2180	VLT/ISAAC	$H$	15×12	17.02±0.10
2003 Feb 26, 09:51	0.2569	UKIRT/UFTI	$K$	9×60	16.39±0.05
2003 Feb 26, 10:04	0.2666	UKIRT/UFTI	$J$	11×60	17.91±0.10
2003 Feb 26, 10:17	0.2746	UKIRT/UFTI	$H$	9×60	17.29±0.10
2003 Feb 26, 12:12	0.3545	UKIRT/UFTI	$K$	9×60	16.69±0.05
2003 Feb 26, 12:23	0.3621	UKIRT/UFTI	$J$	9×60	18.16±0.10
2003 Feb 26, 12:34	0.3698	UKIRT/UFTI	$H$	9×60	17.42±0.10
2003 Feb 26, 18:19	0.6194	Wendelstein	$I$	3×600	19.37±0.07
2003 Feb 26, 19:04	0.6444	Wendelstein	$R$	2×600	19.90±0.05
2003 Feb 26, 19:27	0.6604	Wendelstein	$V$	2×600	20.19±0.06
2003 Feb 26, 19:50	0.6746	Wendelstein	$B$	2×600	20.56±0.07
2003 Feb 26, 22:29	0.7795	JKT	$R$	1×1200	20.22±0.03
2003 Feb 26, 22:43	0.8035	Asiago	$B$	2×1200	21.04±0.03
2003 Feb 26, 23:07	0.8076	NOT/ALFOSC	$V$	1×300	20.67±0.02
2003 Feb 26, 23:13	0.8104	NOT/ALFOSC	$U$	1×600	20.81±0.03
2003 Feb 26, 23:26	0.8298	Asiago	$V$	2×900	20.73±0.02
2003 Feb 26, 23:38	0.8437	Tautenburg	$I$	15×120	20.01±0.08
2003 Feb 26, 23:59	0.8726	Asiago	$R$	2×600	20.44±0.03
2003 Feb 27, 00:43	0.8795	TNG	$U$	1×1200	20.84±0.02
2003 Feb 27, 01:21	0.9153	Tautenburg	$I$	15×120	19.92±0.08
2003 Feb 27, 01:40	0.9201	Asiago	$I$	2×600	20.21±0.03
2003 Feb 27, 02:02	0.9274	JKT	$R$	1×1200	20.57±0.03
2003 Feb 27, 02:35	0.9521	NOT/ALFOSC	$V$	1×300	20.88±0.02
2003 Feb 27, 02:42	0.9587	NOT/ALFOSC	$U$	1×600	21.04±0.04

Table 2—Continued

Date (UT)	$\langle dt \rangle$ (days) <sup>a</sup>	Tel./Instr.	Filter/Grism	Exp. (s)	magnitude
2003 Feb 27, 02:49	0.9677	Wendelstein	<i>I</i>	2×600	20.30±0.14
2003 Feb 27, 03:08	0.9785	Tautenburg	<i>I</i>	5×120	20.46±0.24
2003 Feb 27, 03:12	0.9837	Wendelstein	<i>R</i>	2×600	20.63±0.04
2003 Feb 27, 03:35	0.9993	Wendelstein	<i>V</i>	2×600	21.03±0.06
2003 Feb 27, 03:58	1.0153	Wendelstein	<i>B</i>	2×600	21.33±0.11
2003 Feb 27, 05:04	1.0541	VLT/FORS1	<i>R</i>	1×120	20.64±0.05
2003 Feb 27, 05:05	1.0545	JKT	<i>R</i>	1×1200	20.76±0.05
2003 Feb 27, 05:04	1.0555	NOT/ALFOSC	<i>V</i>	1×300	21.11±0.02
2003 Feb 27, 05:08	1.0580	NTT/SuSI2	<i>B</i>	1×300	21.36±0.03
2003 Feb 27, 05:10	1.0580	VLT/FORS1	<i>R</i> + Wollaston	8×900	...
2003 Feb 27, 05:13	1.0618	NTT/SuSI2	<i>B</i>	1×300	21.37±0.03
2003 Feb 27, 05:11	1.0621	NOT/ALFOSC	<i>U</i>	1×600	21.25±0.05
2003 Feb 27, 05:18	1.0653	NTT/SuSI2	<i>B</i>	1×300	21.48±0.04
2003 Feb 27, 05:25	1.0701	NTT/SuSI2	<i>R</i>	1×300	20.70±0.03
2003 Feb 27, 05:29	1.0729	NTT/SuSI2	<i>R</i>	1×300	20.68±0.03
2003 Feb 27, 05:32	1.0750	NTT/SuSI2	<i>R</i>	1×300	20.84±0.04
2003 Feb 27, 06:14	1.1026	VLT/FORS1	<i>R</i>	1×120	20.79±0.05
2003 Feb 27, 06:28	1.1156	TNG	<i>U</i>	1×600	21.33±0.06
2003 Feb 27, 08:10	1.1885	NTT/SuSI2	<i>B</i>	3×300	21.73±0.03
2003 Feb 27, 07:35	1.1910	VLT/FORS1	600B	5×900	...
2003 Feb 27, 08:27	1.1989	NTT/SuSI2	<i>R</i>	3×300	20.99±0.02
2003 Feb 27, 08:34	1.1997	Tenagra II	<i>I</i>	14×300	20.52±0.10
2003 Feb 27, 09:50	1.2597	UKIRT/UFTI	<i>K</i>	18×60	18.40±0.05
2003 Feb 27, 12:55	1.3962	UKIRT/UFTI	<i>K</i>	36×60	18.69±0.05
2003 Feb 27, 23:49	1.8368	NOT/ALFOSC	<i>V</i>	1×300	22.50±0.07
2003 Feb 27, 23:56	1.8434	NOT/ALFOSC	<i>U</i>	1×600	22.43±0.14
2003 Feb 28, 03:14	1.9851	Wendelstein	<i>R</i>	2×600	21.89±0.13
2003 Feb 28, 04:22	2.0246	TNG	<i>U</i>	3×600	23.02±0.08
2003 Feb 28, 11:47	2.3559	UKIRT/UFTI	<i>K</i>	54×60	19.95±0.08
2003 Mar 02, 04:58	4.0607	VLT/FORS1	<i>B</i>	3×600	24.88±0.06
2003 Mar 02, 05:32	4.0798	VLT/FORS1	<i>V</i>	5×180	24.66±0.09

Table 2—Continued

Date (UT)	$\langle dt \rangle$ (days) <sup>a</sup>	Tel./Instr.	Filter/Grism	Exp. (s)	magnitude
2003 Mar 02, 05:52	4.0937	VLT/FORS1	<i>R</i>	5×180	24.22±0.08
2003 Mar 02, 06:13	4.1083	VLT/FORS1	<i>I</i>	5×180	23.95±0.12
2003 Mar 02, 06:53	4.1472	VLT/ISAAC	<i>K<sub>s</sub></i>	31×10	21.32±0.21
2003 Mar 03, 04:16	5.0753	Gemini South	<i>V</i>	115×60	24.64±0.10
2003 Mar 05, 04:39	7.0500	VLT/FORS1	<i>R</i>	10×180	25.26±0.15
2003 Mar 13, 03:30	15.0156	VLT/FORS1	<i>R</i>	6×600	>26.20

<sup>a</sup>mean observing epoch after the GRB trigger

Table 3: Line identifications<sup>a</sup>

Ion	$f$	Feb 26: FORS2 300 V				Feb 27: FORS1 600 B			
		$\lambda_{\text{obs}}$ (Å)	$z_{\text{abs}}$	$EW_r$ (Å)	$\log N$ ( $\text{cm}^{-2}$ )	$\lambda_{\text{obs}}$ (Å)	$z_{\text{abs}}$	$EW_r$ (Å)	$\log N$ ( $\text{cm}^{-2}$ )
O I $\lambda$ 1302.17	0.049	3859	1.964	$1.2 \pm 0.2$	$15.21^{+0.07}_{-0.08}$	3856	1.962	$0.9 \pm 0.2$	$15.09^{+0.09}_{-0.11}$
		3892	1.989	$2.2 \pm 0.2$	$15.48^{+0.03}_{-0.05}$	3890	1.988	$1.9 \pm 0.3$	$15.41^{+0.07}_{-0.07}$
C II $\lambda\lambda$ 1334.53, 1335.71	0.128,	3952	1.961	$1.1 \pm 0.2$	$14.74^{+0.07}_{-0.09}$	3952	1.961	$1.6 \pm 0.2$	$14.90^{+0.05}_{-0.06}$
	0.115	3983	1.985	$1.8 \pm 0.2$	$14.95^{+0.05}_{-0.10}$	3985	1.986	$2.1 \pm 0.3$	$15.02^{+0.06}_{-0.07}$
Si IV $\lambda$ 1393.75	0.528	4128	1.962	$1.0 \pm 0.1$	$14.04^{+0.04}_{-0.04}$	4126	1.961	$1.0 \pm 0.2$	$14.04^{+0.08}_{-0.09}$
		4155	1.981	$0.9 \pm 0.1$	$14.00^{+0.04}_{-0.05}$	4153	1.980	$1.1 \pm 0.2$	$14.08^{+0.08}_{-0.08}$
Si II $\lambda$ 1526.71	0.127	4522	1.962	$0.9 \pm 0.2$	$14.54^{+0.08}_{-0.11}$	4523	1.963	$1.1 \pm 0.3$	$14.62^{+0.09}_{-0.13}$
		4558	1.986	$1.4 \pm 0.1$	$14.73^{+0.03}_{-0.03}$	4557	1.985	$1.3 \pm 0.3$	$14.70^{+0.09}_{-0.12}$
C IV $\lambda\lambda$ 1548.20, 1550.77	0.191,	4587	1.961	$2.2 \pm 0.2$	$14.73^{+0.04}_{-0.04}$	4585	1.964	$1.1 \pm 0.2$	$14.43^{+0.08}_{-0.08}$
	0.095	4629	1.988	$1.0 \pm 0.1$	$14.39^{+0.04}_{-0.04}$	4625	1.986	$< 0.9$	$< 14.35$
Fe II $\lambda$ 1608.45	0.058	4765	1.963	$0.6 \pm 0.1$	$14.66^{+0.06}_{-0.08}$	4764	1.962	$< 0.8$	$< 14.78$
		4802	1.986	$0.8 \pm 0.1$	$14.78^{+0.05}_{-0.06}$	4802	1.986	$< 1.1$	$< 14.92$
Al II $\lambda$ 1670.79	1.880	4949	1.962	$1.0 \pm 0.2$	$13.33^{+0.08}_{-0.09}$	4952	1.964	$0.7 \pm 0.1$	$13.18^{+0.06}_{-0.07}$
		4989	1.986	$0.9 \pm 0.1$	$13.29^{+0.04}_{-0.05}$	4989	1.986	$1.2 \pm 0.2$	$13.41^{+0.07}_{-0.08}$
Mg II $\lambda$ 2796.35	0.612	5711	1.042	$0.9 \pm 0.1$	$13.33^{+0.04}_{-0.05}$	–	–	–	–
		8284	1.963	$5.0 \pm 0.2$	$14.07^{+0.02}_{-0.02}$	–	–	–	–
		8349	1.986	$6.8 \pm 0.6$	$14.21^{+0.03}_{-0.04}$	–	–	–	–
Mg II $\lambda$ 2803.53	0.305	5726	1.042	$0.5 \pm 0.1$	$13.37^{+0.08}_{-0.09}$	–	–	–	–
		8305	1.962	$3.5 \pm 0.3$	$14.22^{+0.03}_{-0.04}$	–	–	–	–
		8370	1.985	$5.9 \pm 0.4$	$14.44^{+0.03}_{-0.03}$	–	–	–	–

<sup>a</sup>Symbols: oscillator strengths  $f$  (Prochaska et al. 2001), observer-frame wavelengths  $\lambda_{\text{obs}}$ , corresponding absorption redshifts  $z_{\text{abs}}$ , rest-frame equivalent widths ( $EW_r$ ) and deduced column densities ( $N[\text{cm}^{-2}]$ ) of the absorption lines detected in VLT spectra. Typical errors in redshift are  $\pm 0.001$ . Column densities were calculated for the optically thin case. Note that the C II and C IV doublet is not resolved in our spectra. The column densities for these ions refer to the transition with the largest oscillator strength and neglect the other component.